



3 4456 0134873 1

ORNL/TM-8196

ornl

OAK
RIDGE
NATIONAL
LABORATORY

UNION
CARBIDE

Thermal Conductivity of Powders with UO_2 or ThO_2 Microspheres in Various Gases from 300 to 1300 K

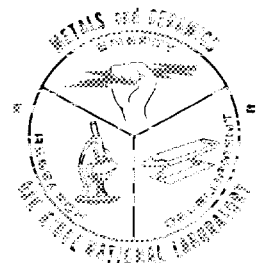
J. P. Moore
R. J. Dippenaar
B. O. A. Hall
D. L. McElroy

OAK RIDGE NATIONAL LABORATORY
CENTRAL RESEARCH LIBRARY
CIRCULATION SECTION
#500N ROOM 175

LIBRARY LOAN COPY

DO NOT TRANSFER TO ANOTHER PERSON.
If you wish someone else to see this report, send in
name with report and the library will arrange a loan.

ORNL-118 (6-97)



OPERATED BY
UNION CARBIDE CORPORATION
FOR THE UNITED STATES
DEPARTMENT OF ENERGY

ORNL/TM-8196
Distribution
Category UC-25

Contract No W-7405-eng-26

METALS AND CERAMICS DIVISION

THERMAL CONDUCTIVITY OF POWDERS WITH UO_2 OR ThO_2 MICROSPHERES
IN VARIOUS GASES FROM 300 TO 1300 K

J. P. Moore, R. J. Dippenaar, R.O.A. Hall, and D. L. McElroy .

Date Published - June 1982

OAK RIDGE NATIONAL LABORATORY
Oak Ridge, Tennessee 37830
operated by
UNION CARBIDE CORPORATION
for the
DEPARTMENT OF ENERGY



3 4456 0134873 1

CONTENTS

ABSTRACT	1
INTRODUCTION	1
MEASUREMENT APPARATUS	2
SPECIMEN DESCRIPTION	7
RESULTS	9
Beds with UO ₂ Microspheres	9
Beds with ThO ₂ Microspheres	13
Comparison of UO ₂ and ThO ₂ Microspheres	16
DISCUSSION OF RESULTS	17
Heat Conduction in Powders Containing Spherical Particles	17
Comparison of Experimental and Calculated Results for Specimens Containing ThO ₂ Particles	19
Comparison of Experimental and Calculated Results for Specimens Containing UO ₂ Particles	25
Relationship of Experimental Results to Use of Microsphere Powders for Reactor Fuel	27
CONCLUSIONS	27
RECOMMENDATIONS	29
ACKNOWLEDGMENTS	29
REFERENCES	29
Appendix A. DETAILS OF SPECIMEN CHAMBER ORNL-1	33
Appendix B. DETAILS OF SPECIMEN CHAMBER ORNL-2	41
Appendix C. MODELS FOR HEAT CONDUCTION IN VIBRATORILY COMPACTED POWDERS WITH SPHERICAL PARTICLES	45
Appendix D. EXPRESSION FOR THE THERMAL CONDUCTIVITY OF A RAREFIED GAS	67
Appendix E	69
Appendix F. NUMERICAL EVALUATION OF THE EFFECTIVE THERMAL CONDUCTIVITY FOR 60.5%- AND 80.5%-DENSE BEDS	73
Appendix G. COMPUTER PROGRAM IN FOCAL LANGUAGE FOR CALCULATING THE THERMAL CONDUCTIVITY OF POWDERS WITH A SINGLE SIZE SPHERICAL PARTICLE	77
Appendix H. COMPUTER PROGRAM IN FOCAL LANGUAGE FOR CALCULATING THE THERMAL CONDUCTIVITY OF POWDERS WITH 440- μ m-DIAM PARTICLES, 44- μ m PARTICLES AND A COMBINATION OF THE TWO SIZES	79

THERMAL CONDUCTIVITY OF POWDERS WITH UO₂ OR ThO₂ MICROSPHERES
IN VARIOUS GASES FROM 300 TO 1300 K

J. P. Moore, R. J. Dippenaar,* R.O.A. Hall,† and D. L. McElroy

ABSTRACT

The thermal conductivities of powders consisting of ThO₂ or UO₂ microspheres in He, Ar, N₂, and Kr were measured by two techniques over a pressure range of 0.03 to 0.6 MPa and a temperature range of 300 to 1300 K. The powders had solid volume packing fractions from 58.5 to 86.6% and were prepared by vibratory compaction and by mixing. The highest thermal conductivity measured was for a powder containing three particle sizes at a packing fraction of 86.6% in helium gas. The applicability of the data to practical reactor fuels is limited to the early stages of fuel burnup because of restructuring.

A theoretical model is derived for heat transfer in powders with spherical particles. This model ascribes the temperature and pressure dependences of the results to limitation of the gas molecule mean free path by the small voids between particles. The model predicts the magnitude of the results obtained in helium to within a few percent when reasonable assumptions are used for the gas-solid accommodation coefficient. Although the model successfully predicts the temperature and pressure dependences of powders with heavier gas molecules (e.g., argon, N₂), the predicted magnitude of λ is low by 20 to 30% because of failure to meet an assumed condition for the calculations.

INTRODUCTION

The thermal conductivity of heterogeneous materials has been of interest for many years because of their many applications and because they are encountered so much in nature. These materials include composites of multiple solids, sands, soils, and powders, which consist of solid particles surrounded by a gas. Powders may consist of particles with spherical, cylindrical, and irregular shapes. Powders formed by vibratory compacting UO₂ or a mixture of UO₂ and ThO₂ microspheres have been of recent interest as fuel for nuclear reactors. In this application, the

*Materials Science Department, University of South Africa, Pretoria.

†Chemistry Division, AERE Harwell, Oxfordshire, England.

thermal conductivity is an important parameter for safe and economic operation and must be accurately known under conditions that are likely to occur during the fuel lifetime.

The present paper presents experimental thermal conductivity results on several powders with spherical UO_2 or ThO_2 particles as functions of temperature and gas phase over a modest range of gas pressure. Gases used included N_2 , He, Ar, and Kr; and particle diameters were from 25 to 1200 μm .

It is desirable to be able to calculate the thermal conductivity of powders and thus avoid the difficulties involved in making experimental measurements on each different powder. This has served as an irresistible lure for many researchers, who have spent extensive time devising models for powder systems. Unfortunately, these models usually do not fit even a limited set of experimental results, much less give assurance that they can be used for predicting thermal conductivity values where no experimental results exist. The best modern review of the various models is by Crane et al.,¹ who concluded that all equation inaccuracies could be attributed to either (1) distorted or unrealistic particle geometry, (2) failure to consider solid-to-solid contact, or (3) invalid assumptions about the heat flow. The third appears to be a universal problem and comes from the necessity of assuming initially that either the isotherms are planes perpendicular to the overall heat flow direction or that the heat flow lines are straight and parallel. An additional problem in many models is that they ignore the lowering of the gas thermal conductivity due to the limitation of the mean free path of the gas molecules by small interparticle spacing. We describe a model that considers both the gas molecule mean free path restriction and radiation transfer in the interparticle voids. The calculated and experimental results have fair agreement for powders with helium in the voids. Agreement for other gases or other particle systems might result from refinements to the model or an improved data base.

MEASUREMENT APPARATUS

All thermal conductivity measurements were made by using a radial heat flow technique that does not require immersion of temperature sensors

directly into the powder bed. This eliminates the large uncertainty regarding location of the temperature sensors at the expense of creating another uncertainty caused by the temperature jump at the specimen boundaries. The general approach is similar to one described by Flynn.² The thermocouples were intercompared in situ by using an "isothermal correction," which is described in Appendix A.

Two markedly different chambers were used for powder containment, and these will be described briefly in the order of their use. The first chamber, henceforth called ORNL-1, is shown in Fig. 1. The powder specimen was vibratorily compacted into the annulus between two stainless steel tubes with outer diameters of 6.35 and 50.8 mm. A regulated direct current was passed through the central tube so that it could be used as a

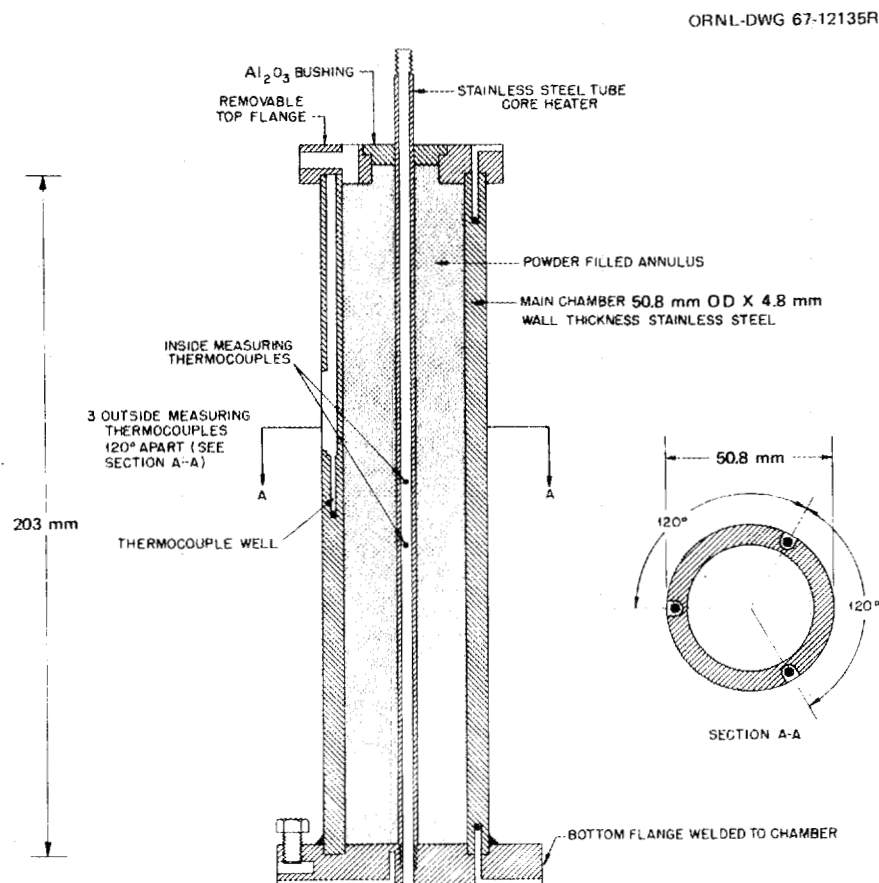


Fig. 1. Cross-sectional view of ORNL-1, showing the specimen annulus between two concentric stainless steel tubes and the positioning of three thermocouples at the midplane in the outer tube.

core heater. Type S thermocouples were positioned along the axis of the core heater and in the walls of the outer chamber to determine temperatures at critical places.

The powder chamber was positioned in a radial heat flow apparatus normally used for measuring the thermal conductivity of solids. This apparatus has been described by Godfrey et al.³ The powder chamber merely replaced the stack of solid disks normally used as a specimen. A three-section muffle heater and top and bottom end guards were used to control the absolute temperature and to control the temperature gradients within the powder chamber to ensure radial heat flow. The control circuits for the heaters and general details of the apparatus are described by Godfrey et al.³

Data were obtained by passing a measured direct current (between 10 and 40 A) through the core heater and adjusting the end guards and muffles until the outer wall of the chamber was isothermal from top to bottom. After the system equilibrated, the current through the core heater and the electromotive forces of the thermocouples inside the core heater and inside the chamber wall were determined. The procedure for calculating the thermal conductivity and further details of ORNL-1 are given in Appendix A. The total determinate error of a thermal conductivity measurement with ORNL-1 is shown in Appendix A to be $\pm 2\%$. Sources of indeterminate error include failure of the inside thermocouples to read the actual temperature of the core heater, nonradial heat flow because of the thick metal at the bottom connecting the inner core heater to the outer wall, and excessive Joule heat at the lower terminal where current was introduced to the core heater. According to the measured temperature profile inside the core heater during testing, the first source should be small. Results of measurements on a quasi-standard MgO powder agreed with results from Godbee⁴ around room temperature but disagreed by as much as -20% at 1300 K.

The second chamber, henceforth referred to as ORNL-2, is shown in Fig. 2. It consisted of two concentric stainless steel cylinders joined at the top by three thin supports and at the lower end by a thin domed ring. An upper tube allowed both the introduction of the sample, which was vibratorily compacted in situ, and the gas phase, the pressure of

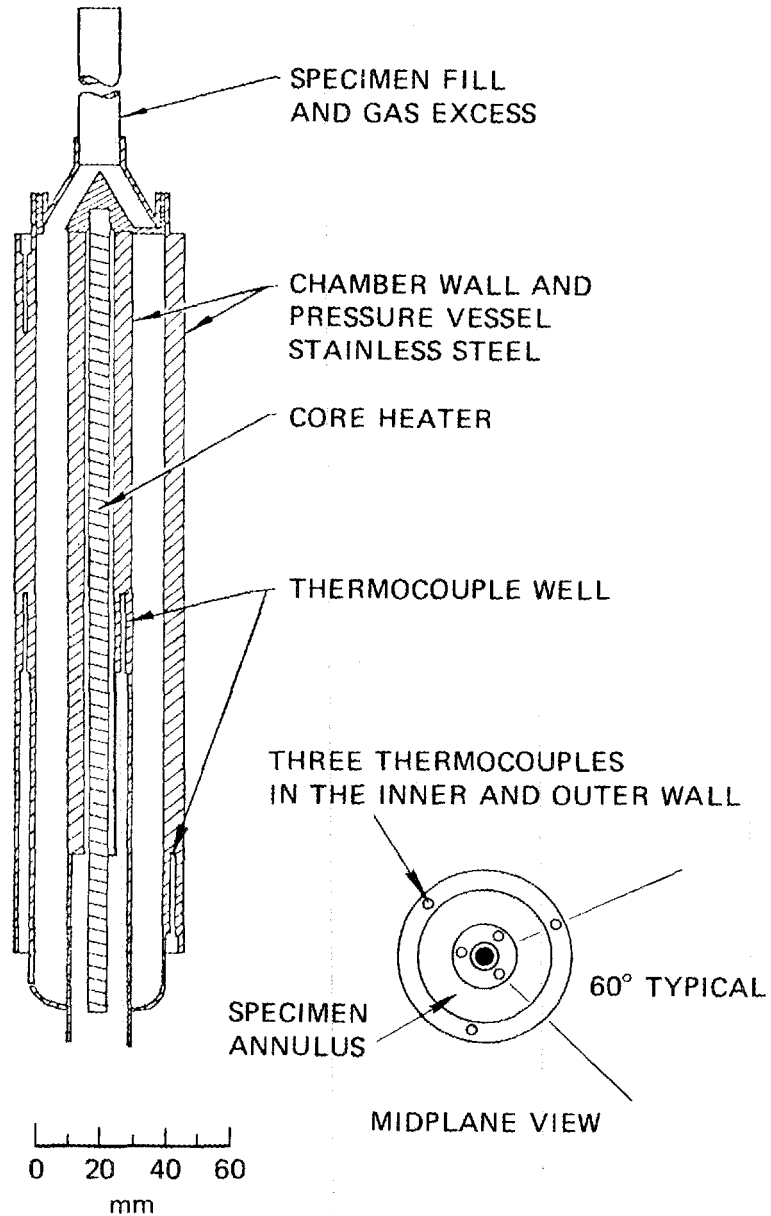


Fig. 2. Cross-sectional view of ORNL-2, showing the specimen annulus between two concentric tubes, the core heater on the central axis of the chamber, and the thermocouple locations.

which was controlled by a self-relieving pressure regulator system not shown in the figure. In ORNL-2, the gas inside the specimen chamber was not in contact with the gas surrounding the chamber. This facilitated changing the gas type and pressure in the powder because only a small volume was involved in any change.

Type S thermocouples were located inside the inner and outer concentric cylinders to determine the temperature drop across the specimen annulus. Details of the central core heater and other aspects of this chamber are given in Appendix B.

In a fashion similar to that described for ORNL-1, this chamber was mounted inside three muffle heaters as shown in Fig. 3. The muffle heaters and environmental chamber surrounding them are normally used to measure the thermal conductivity of solids.

The total determinate error of ORNL-2 is calculated to be $\pm 3.2\%$ in Appendix B. Indeterminate error could have been due to a large temperature drop (relative to that across the specimen) from the "temperature

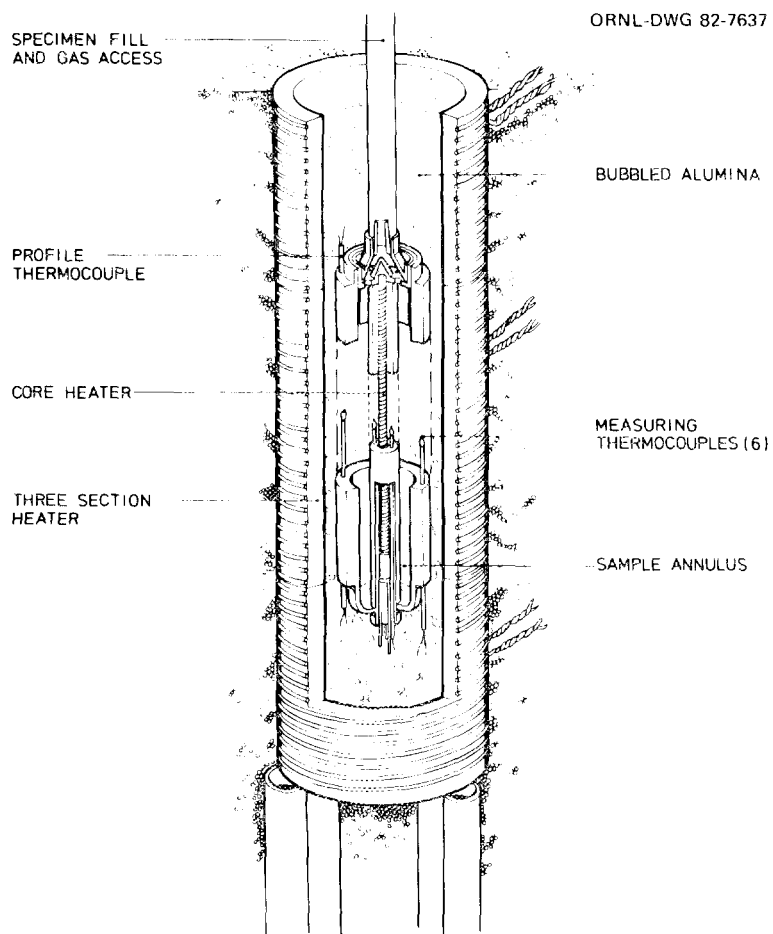


Fig. 3. Cutaway drawing of ORNL-2 installed inside three muffle heaters.

jump" effect at the annulus walls. This is of greater concern for ORNL-2 because of the narrow specimen gap. Extraneous heat flow was examined by using a finite-difference heat-conduction code,⁵ which indicated that measurement errors at 1050 K would be +0.7%, +10.0%, and +20.0% at assumed specimen thermal conductivities of 1.5, 0.7, and 0.3 W/(m·K), respectively. However, measurements were made on the three-particle blended bed of UO₂ (bed 1) with temperature differences up to 25 K between the chamber midplane and ends. These sensitivity measurements, which included appropriate isothermal corrections, showed that temperature imbalance had little influence on the results.

This second chamber, ORNL-2, was probably better than ORNL-1 by virtue of its better length-to-diameter ratio, smaller sample volume, and separate gas system. The latter made it possible to change the gas type and pressure in the specimen annulus without changing that in the regions between specimen chamber and muffle heaters and between muffle heaters and heat sink.

SPECIMEN DESCRIPTION

Seven different powder beds were studied, and these are described in Table 1. All the solid particles were prepared by the "sol-gel" process^{6,7} and carefully examined to eliminate most nonspherical particles and to obtain particles with narrow size distributions. The UO₂ microspheres had a particle density greater than 98% of theoretical. Analysis showed that the primary impurities in the UO₂ microspheres were Fe, Cr, Mn, and Si and that the total of metallic impurities was less than 200 ppm. The fine particles (25–45 μm) had 10 to 20% nonspherical particles, and the medium (280–320 μm) and coarse (1150–1250 μm) particles had less than 5% nonspherical particles. The volume fraction solid of each bed is given in Table 1, and the volume fraction of each particle size is given for the beds (1, 4, 7) containing more than one size.

The gases used in the measurements were taken directly from cylinders of high-purity helium, nitrogen, and argon; krypton was available only in one purity. No attempt was made to further purify the gases before use.

Table 1. Characterization of powder specimens used in this study

Bed	Solid material	Particle sizes (μm)	Volume fraction solid	Measurement chamber used	Gas used	Comment ^a
1	UO ₂	1200 ^b 300 ^c 25-45	0.511 0.173 0.182 <hr/> 0.866	ORNL-2	He, N ₂ , Kr	Blended and poured
2	UO ₂	1200 ^b	0.615	ORNL-2	He	Poured
3	UO ₂	25-45	0.585	ORNL-2	He	Poured
4	UO ₂	1200 ^b 25-45	0.439 0.360 <hr/> 0.799	ORNL-2	He, N ₂	Blended and poured
5	ThO ₂	440	0.64	ORNL-1	He, Ar	VC
6	ThO ₂	<44 ^d	0.64	ORNL-1	He, Ar	VC
7	ThO ₂	440 <44 ^d	0.64 0.20 <hr/> 0.84	ORNL-1	He, Ar	VC ^e

^aVC = Vibratorily compacted; that is, vibrated during loading. Poured beds were vibratorily compacted after loading.

^bParticle sizes between 1150 and 1250 μm .

^cParticle sizes between 280 and 300 μm .

^dMaximum particle diameter was 44 μm , and the mean diameter was about 20 μm .

^eLarge particles vibratorily compacted and then small particles infiltrated by vibration.

The annulus was evacuated and backfilled with the gas three times before any measurements. On one sample of UO₂ microspheres, measurements made in helium after using krypton suggested that this procedure was sufficient to purge the vessel of the previous gas. We used ORNL-1 for the ThO₂ microspheres and ORNL-2 for the UO₂ microspheres.

RESULTS

Beds with UO_2 Microspheres

The thermal conductivities of the three-particle blended bed of UO_2 (bed 1) in helium, nitrogen, and krypton at a pressure of 0.1 MPa are shown in Fig. 4. The relative magnitudes of the three curves reflect the different thermal conductivities of the three gases.

All values were taken during heating cycles except for the value in nitrogen at 559.9 K [$2.023 \text{ W}/(\text{m}\cdot\text{K})$], which was measured after heating to 1071 K and exhibited marked hysteresis. This hysteresis is normally ascribed to the mismatch in the thermal expansion coefficients of the sample and containment, causing a settling of the fine fraction at high temperatures, which results in a compression of the sample at lower temperatures and thus an increased conductivity. However, this increased conductivity was not affected by tapping the outer chamber with a hammer while still at temperature, and the increase could be eliminated by

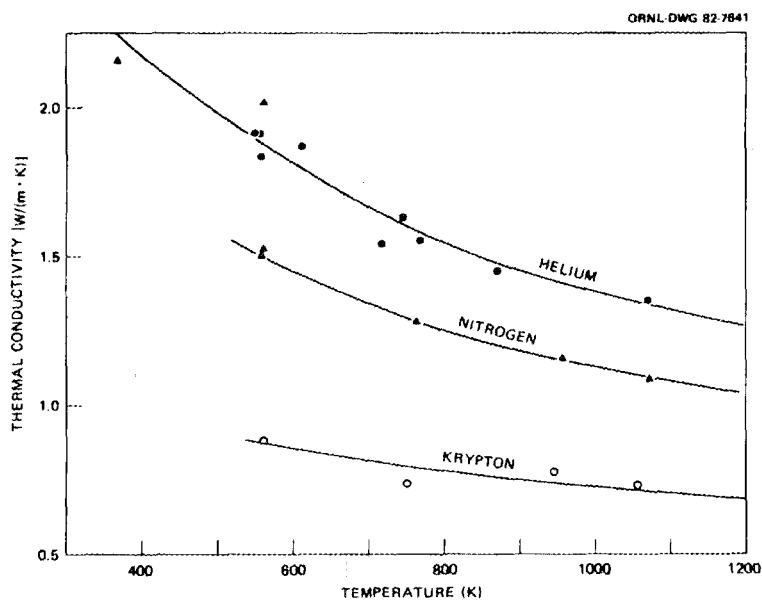


Fig. 4. The thermal conductivity of the three-particle blended bed of UO_2 with a solid fraction of 86.6% (bed 1) in He, N_2 , and Kr versus temperature at a gas pressure of 0.1 MPa.

cooling to room temperature and reheating to 559.1 K, resulting in a value of 1.534 W/(m·K), which agrees excellently with the original curve. The repeat values in helium, after cycling with nitrogen and krypton, agree excellently with the original data, indicating that the bulk sample characteristics were unchanged during the experiment. Too little krypton was available to permit measurement of pressure dependence.

The thermal conductivities of this three-particle bed of UO₂ containing helium or nitrogen are shown versus pressure at fixed temperatures in Fig. 5. All data on this three-particle bed of UO₂ were within 10% of the empirical expression

$$100/\lambda = -2.265 + 0.721(T - 273.15)^{0.6} + 11.75P^{-0.48} \\ + (M - 4.003)[0.4134 + 0.0002T \\ + 0.0033(M - 4.003)] \quad ,$$

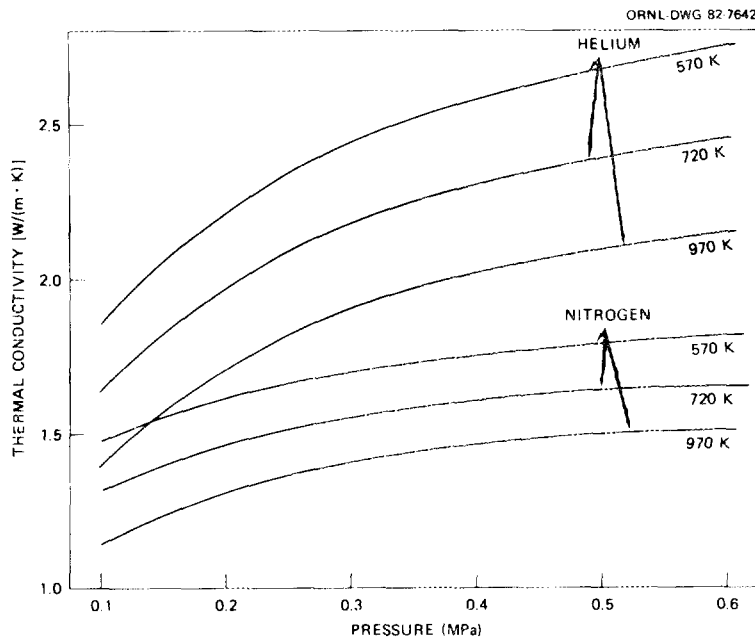


Fig. 5. The thermal conductivity of bed 1 versus gas pressure with helium and with nitrogen in the interparticle voids.

where M is the molecular weight of the gas, T is the absolute temperature in K, P is the pressure in MPa, and λ is the thermal conductivity in $W/(m \cdot K)$.

The thermal conductivity of the two-particle blended bed of UO_2 (bed 4) in helium and in nitrogen at a pressure of 0.1 MPa is shown as a function of temperature in Fig. 6. No data were obtained on this bed in krypton because a failure of a weld in the lower domed ring of the annulus led to premature termination of the experiment. Figure 7 shows that the pressure dependence of the thermal conductivity of this bed is much greater with helium than it is with nitrogen in the voids.

The thermal conductivity of the large-particle poured bed of UO_2 (bed 2) and the small-particle poured bed of UO_2 (bed 3) in helium at a pressure of 0.1 MPa are compared in Fig. 8 with results from beds 1 and 4. The thermal conductivity of the bed with the coarse particles ($1200 \mu m$) increased with increasing temperature, but that with the fine particles ($25-45 \mu m$) decreased. The powder with the fine particles is more sensitive to gas pressure, as shown in Fig. 9.

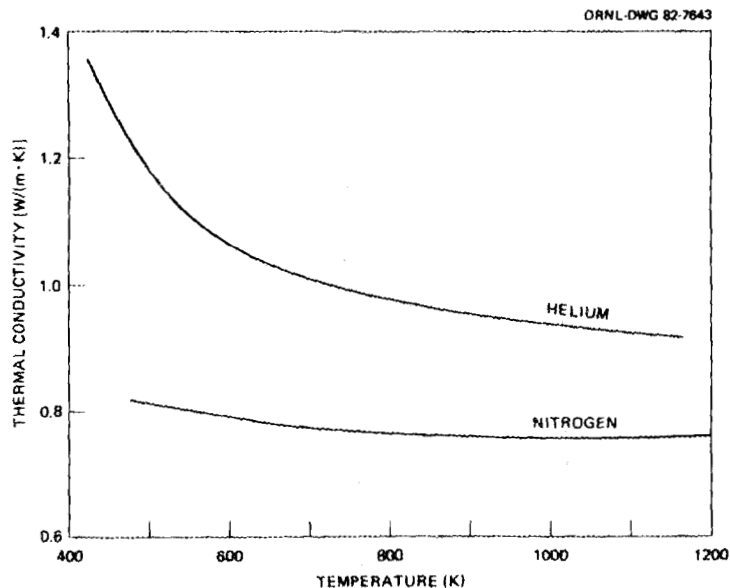


Fig. 6. The thermal conductivity of the two-particle blended bed of UO_2 (bed 4) versus temperature at a gas pressure of 0.1 MPa.

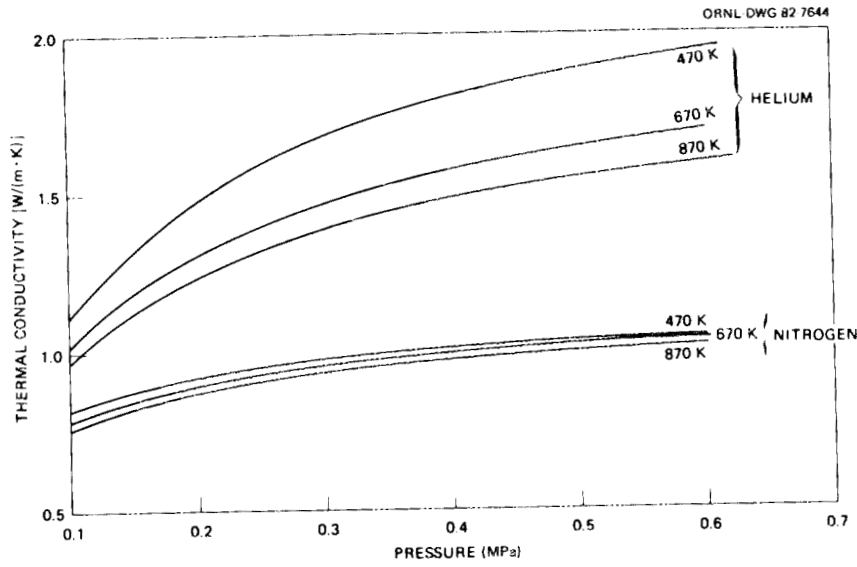


Fig. 7. The pressure dependence of thermal conductivity for bed 4 showing that it is more sensitive to pressure with helium than it is with nitrogen in the interparticle voids.

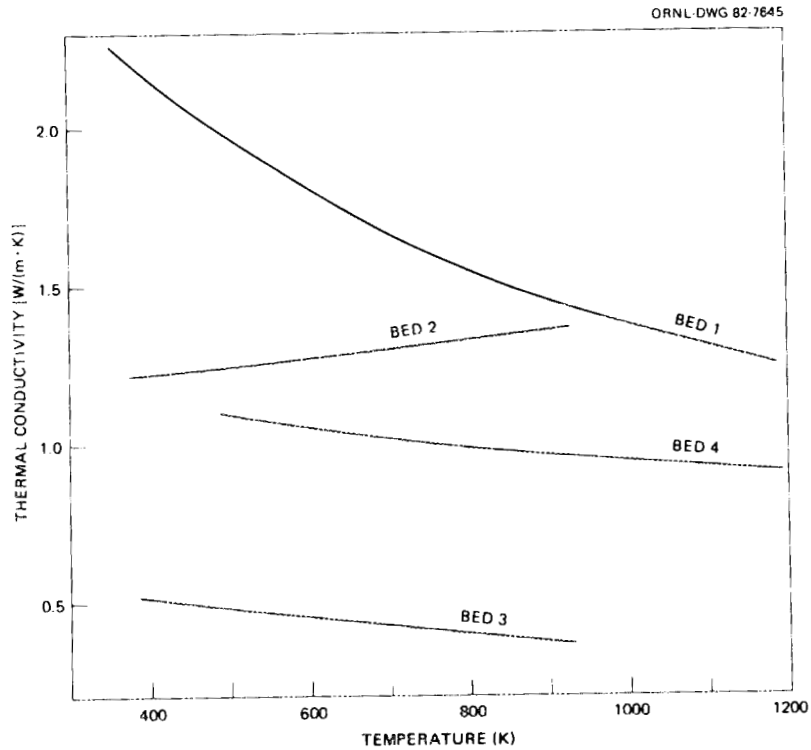


Fig. 8. The thermal conductivity versus temperature for all beds containing UO_2 particles with helium in the voids at a pressure of 0.1 MPa.

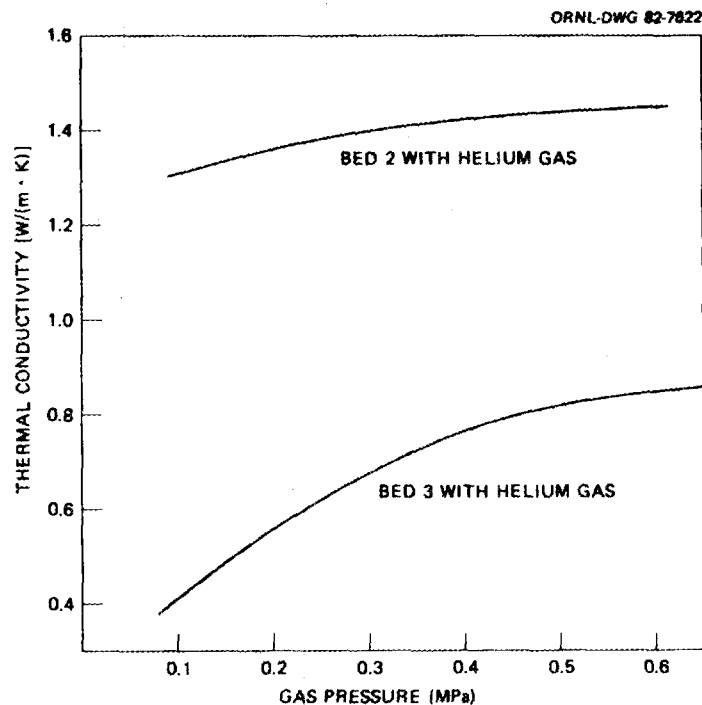


Fig. 9. The thermal conductivity versus pressure of the large-particle bed (bed 2) and small-particle bed (bed 3) of UO_2 at temperatures of 715 and 790 K, respectively, showing that the specimen with the fine particles is more strongly affected by gas pressure.

All thermal conductivity results at 0.1 MPa on the beds containing UO_2 particles have been fitted to low-degree polynomial equations in temperature, and the results are given in Table 2.

Beds with ThO_2 Microspheres

The thermal conductivity results for the three beds containing ThO_2 microspheres are shown versus temperature in Fig. 10 with argon and with helium in the voids between the solid particles at a pressure of 0.1 MPa (~ 1 atm). The thermal conductivities of the large-particle compacted bed of ThO_2 (bed 5) with either argon or helium increase approximately linearly with increasing temperature. Although the bed with the small ThO_2 particles (bed 6) has the same density as the bed with large particles (bed 5), the thermal conductivities of the small-particle bed are much lower for a given gas. The thermal conductivity of this small-particle bed in helium decreases with increasing temperature up to 900 K

Table 2. Results from fitting the measured thermal conductivity at pressures of 0.1 MPa to the function $\lambda = A/T + B + CT + DT^2$. The thermal conductivity is in W/(m·K) and the temperature is in K.

Bed	Bed density and particles	Gas	Upper temperature (K)	A	B	C	D	Variance	Deviation (%)	
									Av	Max
<i>UO₂ microspheres</i>										
1	86.6%, 3 sizes	He	1068		3.108	-0.293 E-5	0.1188 E-5	0.38 E-2	2.18	-5.12
1	86.6%, 3 sizes	N ₂	1072		2.458	-0.215 E-2	0.823 E-6	0.178 E-3	0.63	1.05
1	86.6%, 3 sizes	Kr	1055		1.690	-0.2096 E-2	0.114 E-5	0.22 E-2	2.81	4.55
1	86.6%, 3 sizes	He	768		-2.55	0.146 E-1	-0.12 E-2	Only 3 values put in		
4	79.9%, 2 sizes	N ₂	1098		1.138	-0.84 E-3	0.456 E-6	0.119 E-3	0.646	1.05
4	79.9%, 2 sizes	He	1077	0.467 E-3	0.1817	0.2816 E-6		0.88 E-3	1.646	3.88
2	61.5% 1200 μm	He	878		1.099	0.289 E-3		0.22 E-4	0.257	0.32
3	58.5%, 25-45 μm	He	828		0.6038	0.274 E-3		0.44 E-3	2.62	6.24
<i>ThO₂ microspheres</i>										
5	64%, 440 μm	He	1270		1.106	0.427 E-4	0.26 E-6	0.3 E-3	0.73	1.6
5	64%, 440 μm	Ar	1090		0.2896	-0.2605 E-3	0.509 E-6	0.167 E-9	0.0012	0.003
6	64%, 44 μm	He	1271	0.1288 E+3	0.0765	0.1296 E-3		0.42 E-4	1.01	2.5
6	64%, 44 μm	Ar	1090		0.1634	0.2271 E-4		0.75 E-5	0.89	1.7
7	84%, mixed	He	1273	501.36	0.2713	0.4384 E-3		0.64 E-2	4.22	10.7
7	84%, mixed	Ar	1273		0.8636	-0.585 E-3	0.378 E-6	0.76 E-4	0.71	1.4

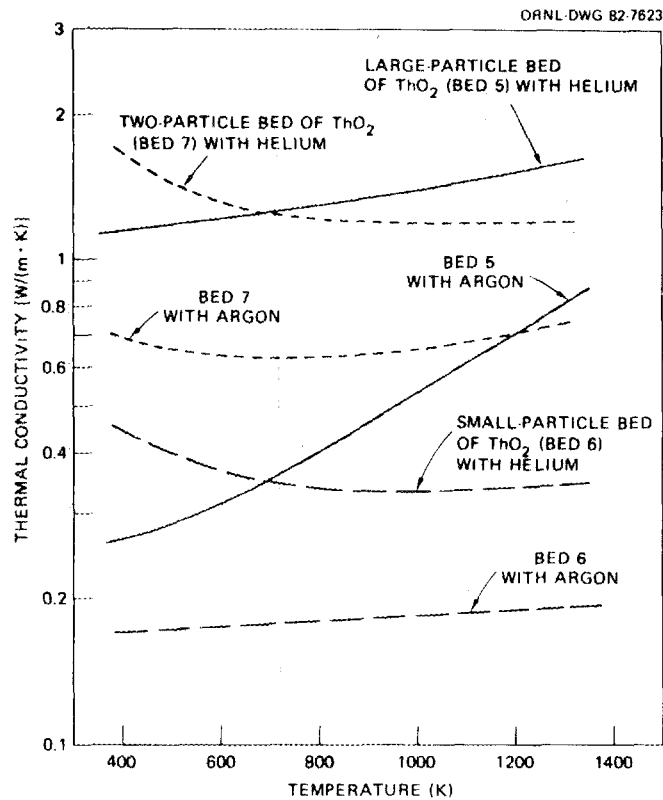


Fig. 10. Thermal conductivity versus temperature of beds containing ThO₂ particles with argon and with helium in the interparticle voids at a pressure of 0.1 MPa.

and increases slightly with temperature above 900 K, whereas that of the same bed in argon increases smoothly over the entire temperature range. These results have been fitted to low-degree polynomial equations, and the results of these fits are given in Table 2.

Figure 11 shows the thermal conductivities of all three beds containing ThO₂ particles (beds 5, 6, 7) in helium and argon versus pressure at fixed temperatures. The thermal conductivity of the large-particle compacted bed of ThO₂ (bed 5) in argon varies by only 5% from 0.06 to 0.19 MPa, but that of the same bed in helium increases by 18% over the same pressure range. The thermal conductivity of the small-particle compacted bed of ThO₂ (bed 6) increases sharply with pressure with either helium or argon in the bed. The pressure dependences of the mixed bed with argon or helium in the voids are between those of the monosize beds.

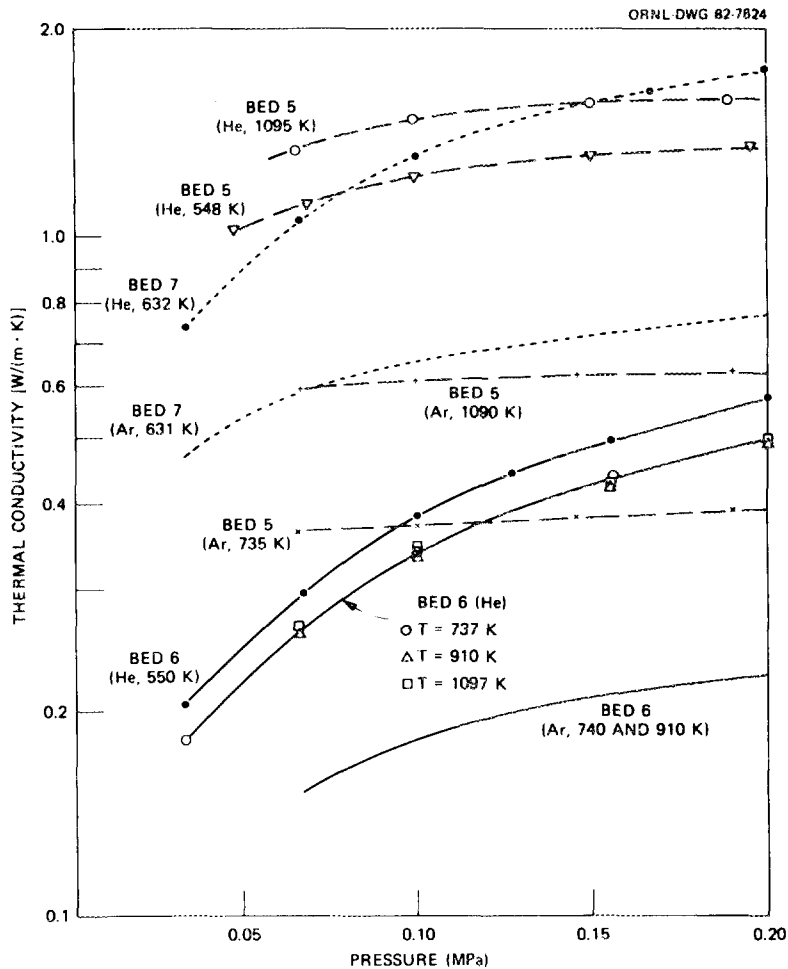


Fig. 11. Thermal conductivity versus temperature of beds containing ThO_2 particles and with helium or with nitrogen in the voids.

Comparison of UO_2 and ThO_2 Microspheres

Since the thermal conductivities of solid UO_2 and ThO_2 are approximately the same at high temperatures,⁸ the results from ORNL-1 on powders containing ThO_2 can be compared with those from ORNL-2 on powders containing UO_2 . Such a comparison is shown in Fig. 12, which shows the thermal conductivities of two UO_2 beds (beds 2 and 3) and two ThO_2 beds (beds 5 and 6) versus helium gas pressure at a common temperature. Because of the chamber design, the data from the UO_2 are at the higher pressure. The results from the small-particle beds of UO_2 and ThO_2 agree to within about 15% over the pressure range of overlap. This difference could be caused by the smaller particles in the UO_2 bed and, hence, a greater limitation

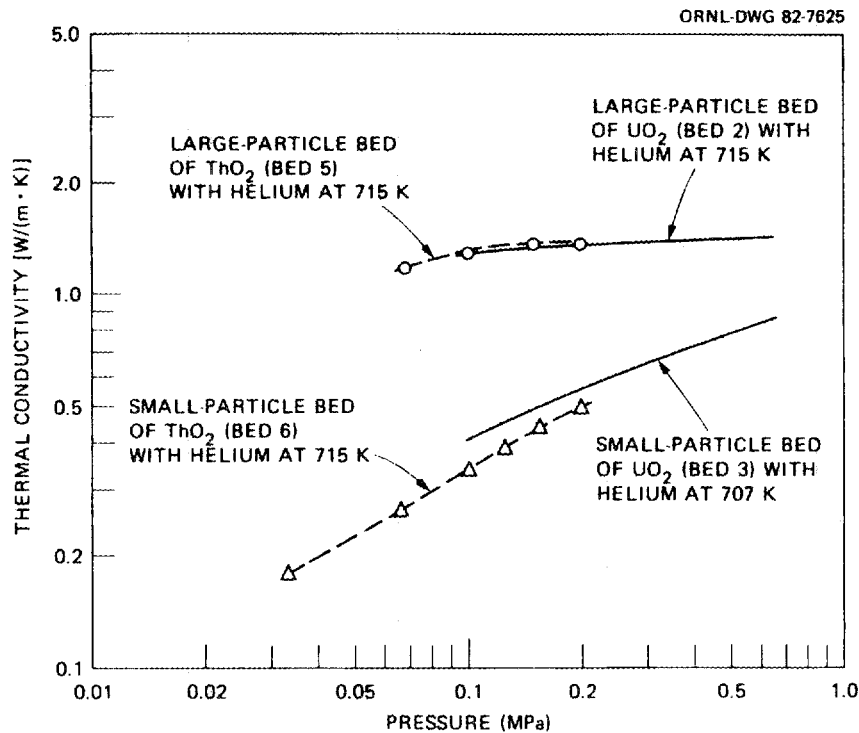


Fig. 12. Comparison of the pressure dependences of results obtained by using ORNL-1 on specimens containing ThO₂ particles and ORNL-2 on specimens containing UO₂.

of the gas mean free paths within the voids between particles. Data shown for the large-particle bed of UO₂ (bed 2) in helium were obtained at 715 K. The results for the large-particle compacted bed of ThO₂ in helium at 715 K were obtained by interpolating between thermal conductivity versus pressure results at 548 and 1095 K. The results on the large particles agree to within 1% over the overlap range, but this may be fortuitous since a little difference in thermal conductivity would be expected from their different void sizes.

DISCUSSION OF RESULTS

Heat Conduction in Powders Containing Spherical Particles

The thermal conductivity of a powder depends on many variables in a complicated manner. These variables include the thermal conductivity of the solid, the gas type, its thermal conductivity in bulk form, its

pressure, the solid fraction, the particle geometry, and the particle sizes. The gas pressure is important because it controls the molecular mean free path of the gas molecules within the interparticle voids. This, in combination with the accommodation coefficient, controls the heat transfer through the voids. Heat conduction by direct particle-particle contact may also have a significant effect.

Attempts have been made in the past to derive models to calculate the thermal conductivity of a gas-powder mixture, and fairly good agreement was found between theory and experiment by a number of investigators: Godbee,⁴ Shimokawa,⁹ Deissler and Eian,¹⁰ and Deissler and Boegli.¹¹ However, when these models are applied to our case, they fail to explain the marked difference in thermal conductivities of the different beds.

In view of the uncertainty and complexity of the parameters that affect the thermal conductivity in such a powder-gas system, a rigorous scientific treatment is not possible at this stage. Our approach is therefore simplified. This model is presented in detail in Appendix C. General assumptions in the model are as follows:

1. The system isotherms are parallel to the bounding planes of the powder beds.
2. A simple hexagonal packing of solid spheres as proposed by Shimokawa⁹ was assumed. This leads to an assumed packing fraction of 0.605, which is close to the values listed in Table 1 for the powders with single-size particles.
3. The model for the two-particle-size powders consisted of a single large particle surrounded by numerous fine particles. The two-particle ThO₂ powder (bed 7) contains 330 fine particles for each coarse particle.
4. The lowering of the gas thermal conductivity due to the limitation of the molecular mean free path was calculated with a model proposed by Kennard.¹²

Appendix C shows that the effect of limiting the gas molecule mean free path (rarefied gas condition) can be expressed in terms of a "temperature jump distance" at the boundaries between solid and gas. This distance depends on the accommodation coefficient, α , for the gas and solid surfaces. The accommodation coefficient, which has a value between 0 and 1, depends on the solid particles, the roughness of the

particle surfaces, and the gas. Since the absolute value of this important coefficient is unknown, it was treated as a variable in the calculations. The model described in Appendix C also includes a term for radiation within the voids. Values for the thermal conductivities of the various powders were calculated from values for the thermal conductivities of solid ThO_2 and UO_2 from Moore et al.⁸ and values for those of the various gases obtained from a compilation of data.¹³

Comparison of Experimental and Calculated Results for Specimens Containing ThO_2 Particles

Experimental and calculated values of the thermal conductivity of the single-particle compacted beds of ThO_2 (beds 5 and 6) in helium are compared in Fig. 13. The calculated thermal conductivity values for the small-particle bed (bed 6) are more sensitive to the assumed α than are those for the large-particle bed (bed 5) because of the smaller voids and,

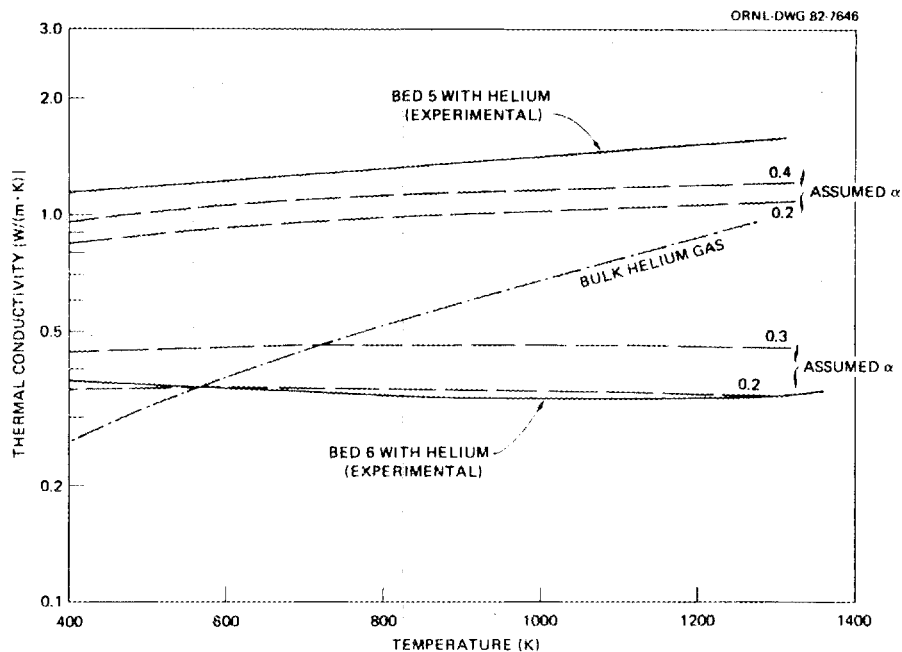


Fig. 13. A comparison of calculated and experimental thermal conductivity values for the large-particle bed 5 and small-particle bed 6 of ThO_2 with helium at a pressure of 0.1 MPa. Calculated curves for two α values are shown for each specimen, and a curve for the thermal conductivity of bulk helium is shown for comparison.

hence, greater limitation of the gas molecule mean free path. For the small-particle bed in helium, calculated values with an assumed α of 0.2 agree well with the experimental values. This same assumed coefficient for the large-particle bed gave results that are about 25% too low. In both cases, however, the calculated and experimental temperature dependences are in nominal agreement. An assumed α of 0.4 would lead to calculated results in better agreement ($\sim 15\%$ at 500 K) with the larger particle bed. This higher value of α would lead to a calculated thermal conductivity for the specimen with small particles that was about 40% too high. However, α may indeed be closer to 0.4, and the calculations with an α of 0.2 fortuitously agree with the experimental results because the powder contained many particles smaller than $44 \mu\text{m}$ (see Table 1). This would lead to experimental values that were too low. Calculations made on the assumptions that the microspheres in the small-particle bed of ThO_2 were $25 \mu\text{m}$ instead of $44 \mu\text{m}$ and that α was equal to 0.4 led to calculated values that are within 10% of the experimental ones over the entire temperature range.

Figure 13 also includes a curve for the thermal conductivity of bulk helium for comparison with the results on powders. Above 600 K, the experimental and calculated values for the small-particle compacted bed of ThO_2 (bed 6) in helium are much less than that of bulk helium even though 64 vol % of the specimen consists of a solid with a thermal conductivity an order of magnitude greater than that of the gas. This illustrates the effect of the poor heat transfer in the rarefied gas between particles. Heat transfer by the helium gas in the larger voids in bed 5 is close to what one would expect with bulk helium, so that the thermal conductivity of bed 5 is much greater than that of bed 6.

We showed earlier that the experimental thermal conductivity of the small-particle compacted bed of ThO_2 (bed 6) was more sensitive to pressure than was that of the large-particle bed (bed 5). The calculated behavior agrees with this, as shown in Fig. 14. This figure also shows that the experimental curves for the large-particle ThO_2 bed (bed 5), which had a solid fraction of 64%, crosses that of the two-particle compacted bed of ThO_2 (bed 7), which had a solid fraction loading of 84%.

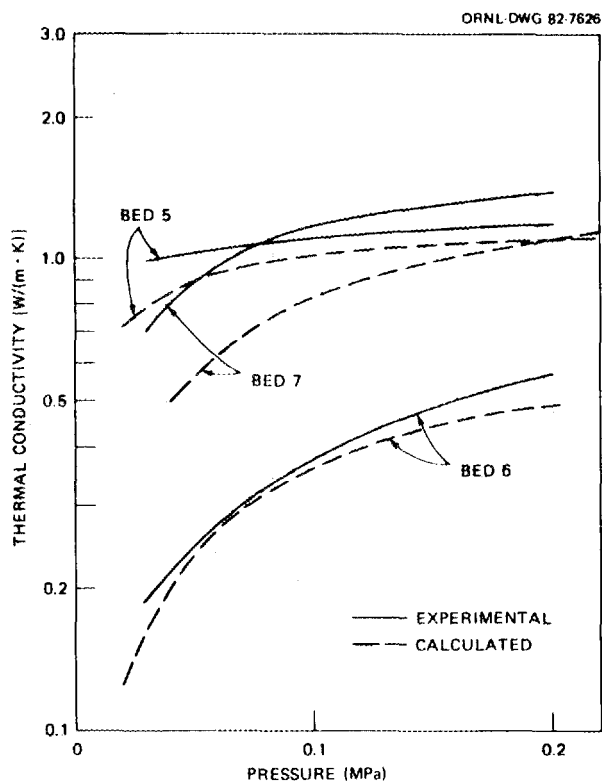


Fig. 14. Experimental and calculated thermal conductivity values for the three beds at 631 K containing ThO_2 (beds 5, 6, and 7) versus helium pressure. Calculated values are for $\alpha = 0.25$.

The calculated curves also show this behavior, although the calculated curves do differ in magnitude from the experimental ones and the curves cross at different temperatures.

Experimental and calculated values for the two beds containing single-size ThO_2 particles with argon in the voids are compared in Fig. 15. The α for argon molecules on the oxide surface would probably be much greater than that for helium molecules,¹² but calculations based on the maximum value for α are still too low for both specimens, although the agreement is within 10% for the small-particle bed of ThO_2 (bed 6) at high temperatures.

A possible explanation for the good agreement between experimental and calculated values in helium and the discrepancy in the case of argon may be found by considering the shape of the isotherms for the two cases. Deissler and Boegli¹¹ have shown that the shape of the isotherms in the

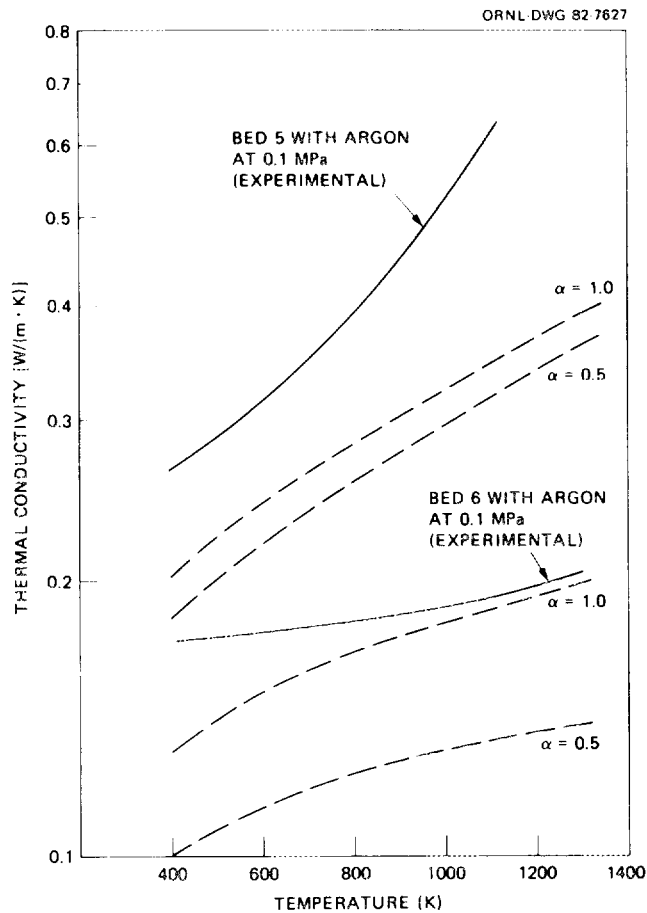


Fig. 15. A comparison of calculated and experimental thermal conductivity values for the large-particle (bed 5) and small-particle (bed 6) of ThO₂ with argon in the voids at a pressure of 0.1 MPa.

unit cell is a function of the ratio of the thermal conductivities of the solid and the gas. Since this ratio is approximately 8 and 70 with helium and with argon, respectively, at 1300 K, the planar isotherm assumption in the model is more valid for helium than for argon.¹⁴ The assumption is also more valid when helium is present in the case of smaller particles for the following reason. Barring mean free path limitation in small voids, most heat flowing through the unit cell described in Appendix C would pass through the solid sphere and through the gas region near the sphere-sphere contact because this would be the most advantageous path for heat flow. In this case, however, the isotherms are far from planar. When the gas mean free path is limited by the small voids around the

contact, the thermal resistance around the contact becomes much greater than that encountered elsewhere, so the heat flow would be reduced. When a powder consists of a 44- μm diam particle surrounded by helium and the mean free path is assumed to be limited by void spacing, the effective thermal conductivity varies by a factor of 2. However, the effective thermal conductivity varies by a factor of 12 for calculations with mean free path unlimited (i.e., with gas with bulk properties in the voids). Heat flow would be more uniform in the former case and the isotherms would be more nearly planar. When the particle size is increased to 440 μm and the mean free path is assumed to be limited, the calculated result falls between the limited and unlimited cases for the 44- μm particle.

Further refinements of the model must consider the influence of deviation of the isotherms from planes that are parallel to the bounding surfaces.

Thus, although the model has some problems, it indicates that the pressure and temperature dependences of the powder thermal conductivities are controlled by the void sizes, which depend on the particle size, and by the limitation of the mean free path within these voids. The influence of the latter on the powder thermal conductivity is shown in Fig. 16 as a function of particle diameter. This figure shows the ratio of the thermal conductivity calculated by the procedure described in Appendix C to calculated values using the same geometrical model but assuming bulk gas properties. This ratio is near unity for powders containing particles with a diameter of 4000 μm and any of the three gases shown but deviates with decreasing particle size until it reaches 0.24, 0.5, and 0.58 at 40 μm with helium, argon, and nitrogen, respectively, in the voids. The influence in helium is greater because helium has a much greater mean free path than does either argon or nitrogen.

In addition to the increasing thermal conductivity with increasing particle size due to the importance of gas molecule mean free path limitation, there is also an increase at elevated temperatures due to a radiation component, which is shown in Fig. 17 as a percentage of the total heat flow. Values for the radiation component were obtained by first calculating total thermal conductivity values with assumed emittances of

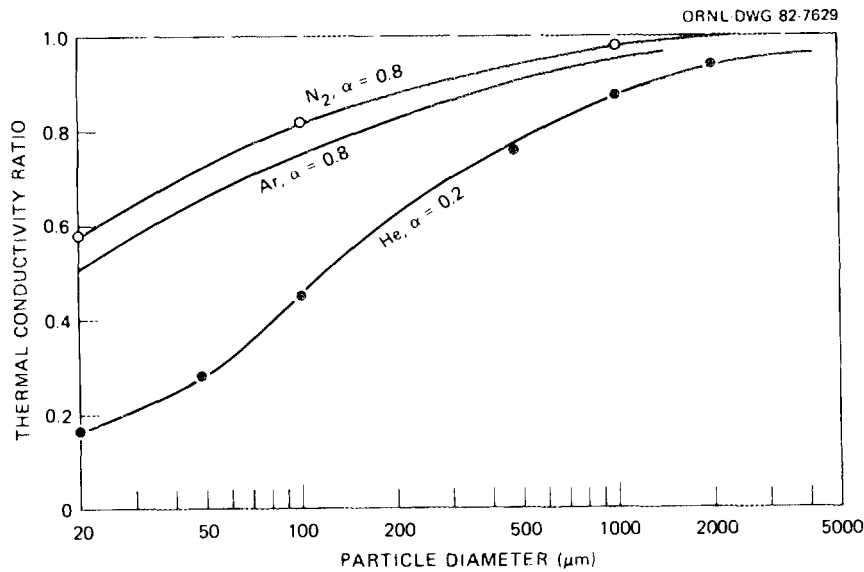


Fig. 16. Ratio of the calculated thermal conductivity of a powder with spherical particles assuming that the gas thermal conductivity is lowered by the temperature jump effect to the value calculated assuming that gas in the voids had bulk gas properties. Calculations are for ThO_2 particles at 1000 K, a gas pressure of 0.1 MPa, an emittance of 0.5, and α values of 0.2, 0.8, and 0.8 for helium, argon, and nitrogen, respectively.

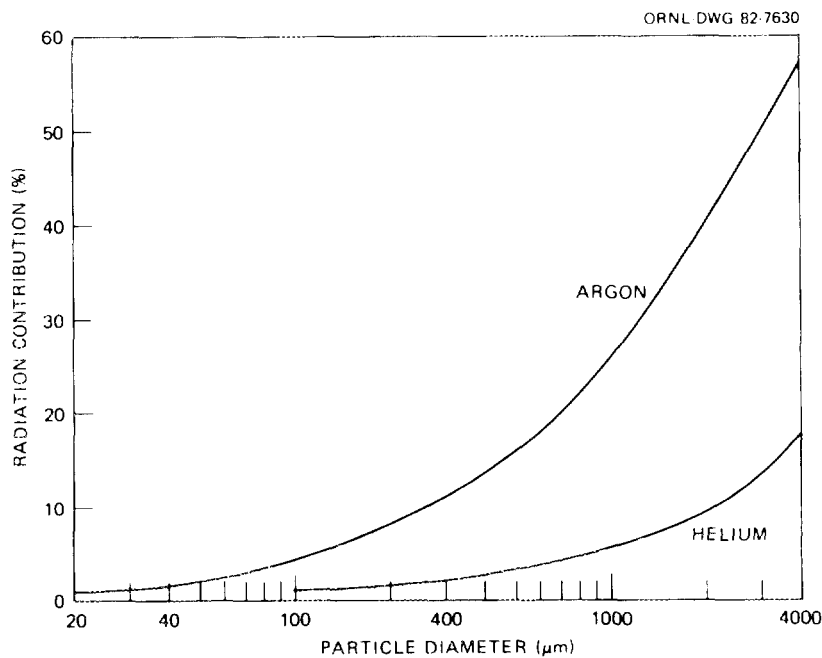


Fig. 17. Percentage contribution of the radiation component to the thermal conductivity of powders with spherical particles as a function of the particle diameter. Parameters were similar to those stated in Fig. 16, and the radiation component was defined as the difference in thermal conductivity calculated with emittance values of 0.5 and 0.0.

0.5 and 0.0 and then calculating the difference between the two results. The absolute magnitude of the radiation component is the same for the two gases but the percentage contribution with argon is a factor of 3 greater than with helium.

Comparison of Experimental and Calculated Results for Specimens Containing UO_2 Particles

The experimental and calculated results for the large-particle bed of UO_2 (bed 2) and the small-particle bed of UO_2 (bed 3) in helium are compared in Fig. 18. Calculations based on an assumed α of 0.35 agree with experimental results on the fine powder specimen (bed 3) to within 10% and agree with results on the coarse powder specimen (bed 2) to within -20%. This value for α describes the experimental pressure dependences, as shown in Fig. 19. The greater influence of pressure on the thermal conductivity of the fine-particle bed (bed 3) is caused by the rarefied gas in the small voids of this material.

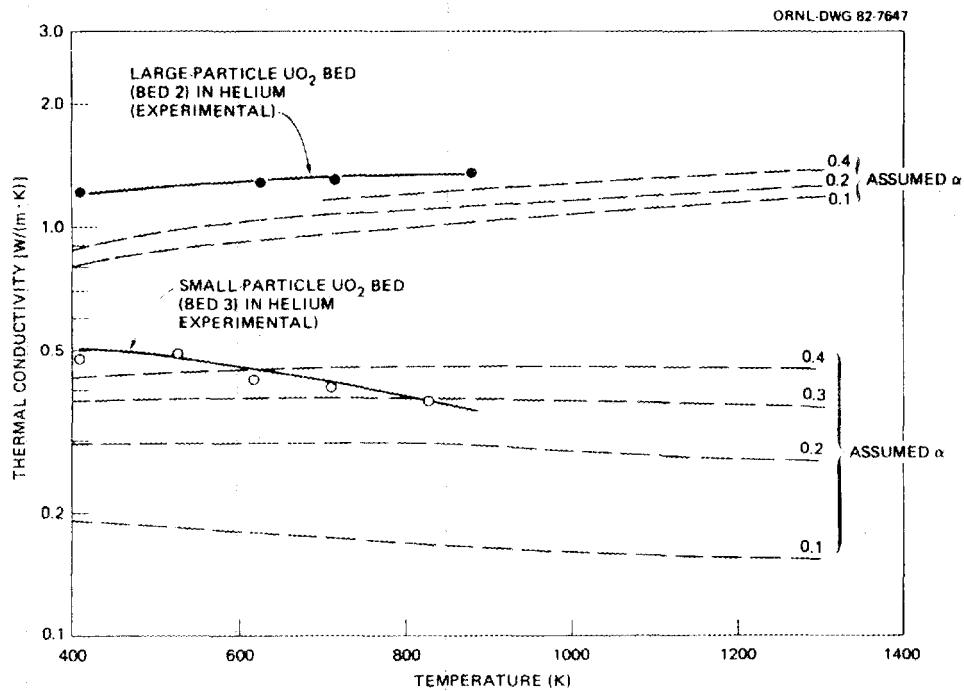


Fig. 18. Experimental and calculated thermal conductivity values for the large- and small-particle beds of UO_2 in helium at a pressure of 0.1 MPa. Calculated curves are for four α values.

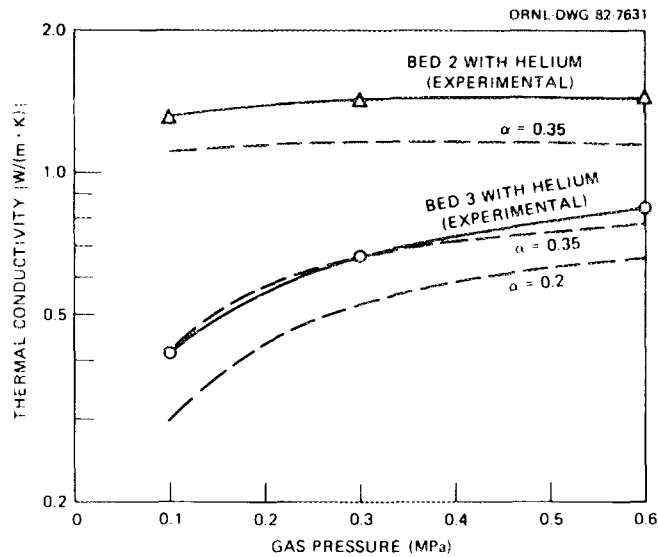


Fig. 19. Experimental and calculated thermal conductivity values for an $\alpha = 0.35$ versus pressure for the large- and small-particle beds of UO_2 containing helium at a temperature of 715 K.

The model described in Appendix C for a two-particle vibratorily compacted bed cannot be used for the two-particle blended bed of UO_2 (bed 4) for two reasons. First, bed 4 has many more fine particles than there are in the model (approximately 10^5 versus 10^2). Second, the large particles in bed 4 consume a much smaller part of the total specimen volume (43.9% versus 64.0%). The first problem could be circumvented by calculating the thermal conductivity of a unit cell consisting of the smaller particles and then assuming that the large particles were in a medium with a thermal conductivity equal to that calculated for the cell containing the small particles. Although the calculation for the cell containing the small particles in helium would be approximately correct, the difference between actual packing of the large spheres (43.9%) and the value assumed in the model (60.5%) is too great to consider the calculations seriously. These results do, however, reflect the same mean free path limitation effects as those described for ThO_2 .

Another finite-difference method has been developed and applied to the results on the three-particle blended bed of UO_2 (bed 1) with helium in the voids.¹⁵ Those calculations use fixed values for the thermal accommodation coefficient of helium on UO_2 surfaces. The assumed¹⁶ values

of α depend on temperature and range from 0.31 at 300 K to 0.23 at 1300 K. These values are reasonably close to the accommodation coefficients that were required to fit our data on single-size powder beds to our model.

Relationship of Experimental Results to Use of Microsphere Powders for Reactor Fuel

Powders consisting of spherical $U_{0.8}Pu_{0.2}O_2$ particles in helium gas have been studied as possible reactor fuels and compared with solid fuels with the same density.^{7,17,18} The results reported herein are only applicable to the early stages of fuel burnup.* This, however, is a critical period in the fuel lifetime because the thermal conductivity is at a minimum and without prior knowledge of the conductivity one might expose the fuel element to conditions under which it is likely to overheat. During reactor operation severe restructuring occurs and raises the thermal conductivity by changing the void space from a continuous gas phase surrounding the spherical particles to lenticular voids and then to long voids parallel to the direction of heat flow. During this restructuring the outer particles remain in good contact with the cladding and prevent the occurrence of a large gap. The absence of this gap leads to an effective thermal conductivity of the powder fuel that is 11% higher than that of a solid fuel.^{17,18} Ades¹⁵ has attempted to calculate the effect of restructuring on the thermal conductivity of sphere-pac UO_2 beds.

CONCLUSIONS

1. Two techniques have been developed for measuring the thermal conductivity of powder from room temperature to 1300 K over a modest pressure range. Experimental results from these two techniques on similar specimens agreed to within 7%. The temperature jump effect at the walls of the apparatus with a small annulus was insignificant and did not influence the data accuracy.

*Although the gas pressure in reactor fuels is greater than the highest pressure attained during measurements on bed 1, Fig. 5 indicates that the thermal conductivity of this bed has nearly saturated at 0.6 MPa.

2. Experimental measurements of the thermal conductivity of powders consisting of opaque, spherical particles of ThO_2 or UO_2 in helium, argon, nitrogen, or krypton have shown the following:

- a. The thermal conductivities of powders with large-diameter particles ($>300 \mu\text{m}$) increase linearly with temperature when the gas pressure is 0.1 MPa ($\sim 1.0 \text{ atm}$). The thermal conductivities of these same powders are relatively insensitive to pressure change.
- b. The thermal conductivity of powders containing small particles (either powders with only small particles or with mixed particle sizes) are temperature independent at 0.1 MPa with the heavier gases such as argon and nitrogen in the voids and have a negative temperature dependence with helium in the voids. Helium provides a positive temperature dependence at higher pressures. These powders also exhibit strong pressure sensitivity, with the greatest sensitivity occurring with helium in the voids.
- c. The highest thermal conductivity measured was for a powder with three different sizes of UO_2 particles in helium.

3. A theoretical model was developed for describing heat transfer in powders with spherical particles. This model

- a. describes the temperature and pressure dependence of the thermal conductivity of most of the specimens studied experimentally,
 - b. attributes most of the behavior of powders with small particles to limitation of the gas mean free path by small voids in the powder,
 - c. shows that the radiation component of the thermal conductivity is a strong function of particle size and is about 5 or 26% of the total when helium or argon, respectively, is in the interparticle voids of a powder with $100\text{-}\mu\text{m}$ particles,
 - d. agrees with experimental results on powders containing argon or with small-particle beds containing helium. This is attributed to the more nearly planar isotherms for these systems.
4. The applicability of these data to reactor fuels is limited to the early stages of fuel burnup because of restructuring.

RECOMMENDATIONS

The theoretical model for heat transfer should be modified, if possible, to take into account the fact that isotherms are not always planes parallel to the bounding surfaces of the powder. In addition, thermal conductivity should be measured on powders with small spherical particles (<100 μm in diameter) with a narrow size distribution to test the theoretical model.

A powder of opaque microspheres would make an excellent thermal conductivity standard in the low thermal conductivity range because proper selection of interparticle gas and gas pressure would give a wide range of thermal conductivity values. In addition, one could come much closer to reproducing a specific solid fraction loading with all particles spherical and the same size than one could with irregularly shaped particles with a wide size distribution. Therefore, careful measurements should be made on a plentiful powder of this type to establish a good thermal conductivity standard in the low thermal conductivity range.

ACKNOWLEDGMENTS

We gratefully acknowledge R. S. Graves and F. J. Weaver for providing assistance and taking some of the experimental data, S. Peterson for editorial assistance, and S. G. Frykman for preparing the report for publication. R.O.A. Hall and R.J. Dippenaar, would like to thank the Metals and Ceramics Division of Oak Ridge for courtesies extended during our visits.

REFERENCES

1. R. A. Crane, R. I. Vachon, and M. S. Khader, "Thermal Conductivity of Granular Materials -- A Review," pp. 109-23 in *Proc. 7th Symp. Thermophysical Properties* (held at NBS, Gaithersburg, Md., 1977), A. Cezairliyan, ed., American Society of Mechanical Engineers, New York, 1977.

2. D. R. Flynn, "A Radial Flow Apparatus for Determining the Thermal Conductivity of Loose-Fill Insulations to High Temperature," *J. Res. Natl. Bur. Stand. Sect. C* 67(2): 129 (April-June 1963).
3. T. G. Godfrey, W. Fulkerson, T. G. Kollie, J. P. Moore, and D. L. McElroy, *Thermal Conductivity of Uranium Dioxide and Armco Iron by an Improved Radial Heat Flow Technique*, ORNL-3556, June 1964.
4. H. W. Godbee, *Thermal Conductivity of Magnesia, Alumina, and Zirconia Powders in Air at Atmospheric Pressure from 200°F to 1500°F*, ORNL-3510, April 1966.
5. W. P. Turner, P. C. Elrod, and I. I. Siman-Tov, *HEATING5 — An IBM 360 Heat Conduction Program*, ORNL/CSD/TM-15, March 1977.
6. R. G. Wymer, *Laboratory and Engineering Studies of Sol-Gel Processes at Oak Ridge National Laboratory*, ORNL-TM-2205, May 1968.
7. F. G. Kitts, R. B. Fitts, and A. R. Olsen, "Sol-Gel Urania-Plutonia Microsphere Preparation and Fabrication into Fuel Rods," pp. 195-210 in *Int. Symp. Plutonium Fuels Technol., Scottsdale, Ariz., 1967*, *Nucl. Met.* 13, K. E. Horton, R. E. Machevey, and R. J. Allio, eds., American Institute of Mining, Metallurgical, and Petroleum Engineers, New York, 1968.
8. J. P. Moore and D. L. McElroy, "Thermal Conductivity of Nearly Stoichiometric Single-Crystal and Polycrystalline UO_2 ," *J. Am. Ceram. Soc.* 54: 40-46 (1971).
9. J. Shimokawa, *Deionizing Processes with Ion Exchange and with Electromigration*, JAERI-1038, Japan Atomic Energy Research Institute, Tokyo, June 30, 1962.
10. R. G. Deissler and C. S. Eian, *Investigation of Effective Thermal Conductivities of Powders*, NACA-RM-E-52C05, National Advisory Committee for Aeronautics, Cleveland, June 24, 1952.
11. R. G. Deissler and J. S. Boegli, "An Investigation of Effective Thermal Conductivities of Powders in Various Gases," *Trans. ASME* 80: 1417-25 (1958).
12. E. H. Kennard, *Kinetic Theory of Gases*, McGraw-Hill, New York, 1938.
13. *Thermophysical Properties Research Center Data Book*, Vol. 2, Purdue Research Foundation, Lafayette, Ind., 1964.

14. K. L. Peddicord and M. J. Ades, "Prediction of the Thermal Conductivity of Sphere-Pac Fuel," *Trans. Am. Nucl. Soc.* 28: 552 (1978).
15. M. J. Ades, *Thermal Conductivity of Sphere-Pac Fuel*, DOE/ET/34215-26, Exxon Nuclear Co., Inc., Richland, Wash., July 1981.
16. A. Ullman, R. Acharya, and D. R. Olander, "Thermal Accommodation Coefficients of Inert Gases on Stainless Steel and UO₂," *J. Nucl. Mater.* 51: 277-79 (1974).
17. R. B. Fitts and F. L. Miller, "A Comparison of Sphere-Pac and Pellet (U,Pu)O₂ Fuel Pins in Low-Burnup Instrumented Irradiation Tests," *Nucl. Technol.* 21: 26-38 (1974).
18. A. R. Olsen, R. B. Fitts, and W. J. Lackey, "In-Reactor Restructuring Temperatures and Kinetics for (U,Pu)O₂," pp. 579-602 in *Proc. Conf. Fast Reactor Fuel Element Technology*, R. Farmakes, ed., American Nuclear Society, Hinsdale, Ill., 1971.

Appendix A

DETAILS OF SPECIMEN CHAMBER ORNL-1

The specimen chamber for ORNL-1, which is shown in Fig. 1, was fabricated from a 50.8-mm-OD by 4.13-mm-ID by 203.2-mm-long stainless steel tube. A bottom flange was welded to this tube and a removable flange was positioned on the top. A type 304L stainless steel tube with an outer diameter of either 3.175 or 6.35 mm formed the core heater, and it was threaded into the bottom flange and passed through an Al₂O₃ bushing in the top flange. Dimensional tolerance on the flanges and bushing was controlled to ensure central location of the core heater to within #0.15 mm. Holes in the top flange permitted control of the gas type and pressure inside the powder annulus. The nominal volume of this annulus was 0.27 L. This specimen chamber was placed inside an environmental chamber normally used for measuring the thermal conductivities of solids.

All temperature measurements were made with type S thermocouples consisting of 0.25-mm-diam wires of Pt-10% Rh and platinum insulated with two-hole high-purity Al₂O₃ tubing. Three thermocouples were spaced 120° apart in the outer chamber wall in the central plane of the cylinder. The thermocouple wells in the chamber wall were 20 mm deep and 1.6 mm diam, and the hot junction was centered inside a 1.6-mm-diam one-hole Al₂O₃ tube at the bottom of the well. This configuration ensured a snug fit between thermocouple and well in addition to placing the first 20 mm of the thermocouple wire in an isothermal region. This prevented heat flow away from (or toward) the thermocouple hot junction. Two thermocouples were insulated with 1.6-mm-diam tubing and inserted into the central core heater near the cylinder central plane. One of these thermocouples entered from the core heater top and one from the bottom. In addition to the measuring thermocouples just described, two thermocouples at each end of the chamber wall monitored the temperature profile along the cylinder wall. This cylinder wall was kept isothermal for each datum by adjusting the temperatures of the various heaters surrounding the specimen chamber.

When the system reached equilibrium, all thermocouple emfs and the voltage drop across a standard resistor wired in series with the core heater were measured with a potentiometer. The thermocouple emfs were converted to temperatures, and the thermal conductivity was calculated with

$$\lambda = \frac{q'}{2\pi} \frac{\ln(r_3/r_2)}{T(r=0) - T(r_4) - \Delta T_{\text{iso}} - \frac{q'}{2\pi\lambda_{\text{ss}}} \left(\ln \frac{r_2}{r_5} + \ln \frac{r_4}{r_3} \right)} \quad (\text{A1})$$

where

- $T(r=0)$ = the average temperature indicated by the thermocouples in the core heater,
- $T(r_4)$ = the average temperature indicated by the thermocouples in the outer chamber wall,
- r_2 = the outer core heater radius,
- r_3 = the inner radius of the outer stainless steel tube (i.e., the outer radius of the specimen annulus),
- r_4 = the distance between the center of the core heater and the thermocouple wells in the outer chamber wall,
- r_1 = inside radius of the core heater,
- r_5 = $\exp[(\ln r_2 + \ln r_1)/2]$,
- q' = the power per unit length dissipated by the core heater,
- λ_{ss} = thermal conductivity of the core heater and chamber wall, and

ΔT_{iso} is an internal calibration of the thermocouples, which was obtained with the electrical current in the core heater at zero and the chamber near isothermal conditions.

The use of the ΔT_{iso} as a correction for small spurious emfs has been discussed by others.¹ The term in the denominator containing $\ln(r_2/r_5)$ and $\ln(r_4/r_3)$ is a correction for the temperature drops between the inner and outer specimen radii and the thermocouple hot junctions in the stainless steel walls.

The thermal conductivity of the stainless steel core heater and chamber wall was determined by measuring their electrical resistivity

versus temperature and using an equation by Powell² that relates the electrical resistivity and thermal conductivity. The heat generated per unit length by the core heater was calculated by

$$q' = I^2 R/l ,$$

where I was the current flow through the core heater and R/l was the resistance per unit length determined by measuring the voltage drop between potential taps with a known spacing. The temperature near the potential taps was measured with a thermocouple. The distance between the potential taps was determined by comparison with knife edges of known spacing. A relation between R/l for the core heater and temperature was carefully established by passing small currents through the core at various temperatures between 300 and 1300 K. This approach eliminated the need for placing potential taps on the core heater inside the powder and simplified the assembly without adding significant error.

The fractional uncertainty in a thermal conductivity measurement using ORNL-1 can be written as

$$\left| \frac{\Delta \lambda}{\lambda} \right| = \left| \frac{\Delta q'}{q'} \right| + \left| \frac{\Delta r_3}{r_3 \ln(r_3/r_2)} \right| + \left| \frac{\Delta r_2}{r_2 \ln(r_3/r_2)} \right| + \left| \frac{\Delta [T(r=0) - T(r_4) - C']}{T(r=0) - T(r_4) - C'} \right| , \quad (A2)$$

where $C' = (q'/2\pi\lambda_{SS})[\ln(r_2/r_5) + \ln(r_4/r_3)]$. This equation would indicate a total determinate error of $\pm 2\%$ for either size core heater.

Two primary sources of indeterminate error occur in the measurements. The first of these is the "temperature jump" effect between the specimen and adjacent metal walls. Equation (A1) assumes that the temperature

drop at these surfaces is negligibly small. The magnitude of the error caused by this assumption can be calculated approximately and checked experimentally.

The temperature drop that occurs at a solid-gas interface is written by Kennard³

$$T_K - T_W = G \frac{\partial T}{\partial n}, \quad (\text{A3})$$

where T_W is the solid wall temperature and T_K is the temperature that the gas would have if the temperature gradient in the gas normal to the wall, $\partial T/\partial n$, continued without change to the wall surface. The constant G can be approximated by

$$G = \frac{2 - \alpha}{\alpha} \frac{2}{\gamma + 1} \frac{\lambda_g}{\eta C_v} \Lambda, \quad (\text{A4})$$

where

- α = accommodation coefficient of the gas-wall interface,
- λ_g = thermal conductivity of the bulk gas,
- η = viscosity of the gas,
- C_v = specific heat of the gas at constant volume,
- Λ = mean free path of the gas molecules,
- γ = the ratio of C_p to C_v . (C_p = specific heat at constant pressure.)

The temperature drop is then

$$T_K - T_W = \frac{2 - \alpha}{\alpha} \frac{2}{\gamma + 1} \frac{\lambda_g}{\eta C_v} \Lambda \frac{\partial T}{\partial n}. \quad (\text{A5})$$

Since $\partial T/\partial n$ for the radial apparatus is given by

$$\frac{\partial T}{\partial n} = \frac{\partial T}{\partial r} = \frac{q'}{\lambda_g 2\pi r}, \quad (\text{A6})$$

Eq. (A5) becomes

$$T_K - T_W = \frac{2 - \alpha}{\alpha} \frac{\Lambda q''}{(\gamma + 1) \eta C_v \pi r} \quad (A7)$$

The most significant aspect of this equation is the inverse relation between $T_K - T_W$ and the surface radius. This means that the "temperature jump" effect at the inner radius of the specimen exceeds that at the outer radius. The combined error T_j would be

$$T_j = \frac{2 - \alpha}{\alpha} \frac{\Lambda q''}{(\gamma + 1) \eta C_v \pi} \left(\frac{1}{r_3} + \frac{1}{r_2} \right) \quad (A8)$$

and the percentage error caused by the temperature jump effect would be

$$\% \text{ error} = 100 \frac{T_j}{\delta T} = \frac{100}{\delta T} \frac{2 - \alpha}{\alpha} \frac{\Lambda q''}{(\gamma + 1) \eta C_v \pi} \left(\frac{1}{r_3} + \frac{1}{r_2} \right) \quad (A9)$$

The accommodation coefficient is a measure of the efficiency of heat transfer between a surface and the gas in contact with the surface. This coefficient can vary from about 0.05 to 1.0 depending on the surface material and finish and the gas type.⁴ The surfaces bounding the powder bed were slightly oxidized stainless steel, which has a high accommodation coefficient, but for calculation we shall assume a pessimistically low value of 0.1. Values for γ , $\lambda_g/\eta C_v$, Λ , and λ_g were obtained from Kennard,³ Tsederberg,⁴ and the TPRC data compilations.⁵

Calculations suggest that the error should be less in magnitude than -0.67% and -0.96% for core heaters with diameters of 3.175 and 6.35 mm, respectively. Thus, the error would depend on the core heater size, and measurements using different size core heaters would yield different results if the error was significant. Measurements using the two core heaters above indicated that this error was small.

Calculation of the thermal conductivity using Eq. (A1) requires the assumption that the system is infinitely long. Failure of the system to meet this assumption leads to nonradial heat flow at the specimen

midplane, which, in turn, leads to an error not included in Eq. (A2). To assess this indeterminate error, the system was thermally analyzed by using a finite-difference heat conduction code in a manner described by Godfrey et al.⁶ This analysis showed that the maximum error due to this source would be about +8% and would occur for the powder specimens with a thermal conductivity near 0.2 W/(m·K). This error is approximately proportional to the reciprocal of the specimen thermal conductivity and would thus be much less than +8% for most of the results presented for powders containing ThO₂. This error was due primarily to the fact that the lower end of the core heater was in good thermal contact with the outer chamber wall and usually had about the same temperature as the outer wall, which was adjusted to be isothermal. This placed a temperature gradient on the core heater, which caused heat to flow axially away from the center of the core heater and thus lead to positive errors. This chamber would have been much better had the need for vibratory compaction not prevented the threaded connection at the bottom of the core heater from being replaced with an oxide bushing similar to the one shown at the top.

This system was tested with an MgO powder with a density 58% of theoretical. Although the results were only a few percent below those obtained by Godbee⁷ at room temperature, results at 1300 K were about 20% below Godbee's values, even after a negative correction of 10% was applied to his high-temperature data. This correction was necessary because a heat shunting error in his data was discovered after publication. The cause of the remaining 20% discrepancy is unknown, but it is probably due to experimental error with ORNL-1 and possibly slight differences in powder densities.

References

1. M. J. Laubitz and D. L. McElroy, "Precise Measurements of Thermal Conductivity at High Temperatures (100–1200 K)," *Metrologia* 7(1): 1–15 (1971).
2. R. W. Powell, "Thermal Conductivities of Some Gas-Turbine Materials," *Iron Steel Inst. London Spec. Rep.* (43): 315–18 (1952).

3. E. H. Kennard, *Kinetic Theory of Gases*, McGraw-Hill, New York, 1938.
4. N. V. Tsederberg, *Thermal Conductivity of Gases and Liquids*, The Massachusetts Institute of Technology Press, Cambridge, Mass., 1964.
5. *Thermophysical Properties Research Center Data Book*, Vol. 2, Purdue Research Foundation, Lafayette, Ind., 1964.
6. T. G. Godfrey, D. L. McElroy, and Z. L. Ardary, "Thermal Conductivity of Oriented Fibrous Carbon Insulation from 300 to 1300 K in Nitrogen and Argon at One Atmosphere," *Nucl. Technol.* 22: 94-107 (1974).
7. H. W. Godbee, *Thermal Conductivity of Magnesia, Alumina, and Zirconia Powders in Air at Atmospheric Pressure from 200°F to 1500°F*, ORNL-3510, April 1966.

Appendix B

DETAILS OF SPECIMEN CHAMBER ORNL-2

The specimen chamber designated ORNL-2 and shown in Fig. 2 consisted of two concentric stainless steel tubes attached so that the powder specimen would fill the annulus between the tubes. The inner diameter of the outer tube and the outer diameter of the inner tube were 40.16 mm and 19.12 mm, respectively, which led to a specimen gap of 10.52 mm. The height of the powder specimen in the annulus was 223 mm. A thin domed ring at the bottom of the annulus connected the two tubes and served as the bottom of the specimen chamber. The strength of this domed ring limited the upper pressure of this chamber to 0.6 MPa at an upper temperature of 1000 K.

The core heater, which is shown in Fig. B1, consisted of a platinum wire noninductively wound on a grooved ceramic support. The distance between potential taps attached to the platinum wire was measured with a traveling-stage microscope. This assembly was inserted into the inside of the inner stainless steel tube so that it was at the central axis of the chamber.

Platinum and Pt-10% Rh thermocouple wire (0.25 mm diam) was annealed to remove the strain during manufacture, and thermocouples fabricated from this wire were inserted into the long thermocouple wells in the chamber. The close fit between the thermocouple insulation and the long depth of immersion minimized the temperature gradient at the thermocouple hot junction. Six thermocouples, three in the inner cylinder and three in the outer cylinder, were positioned in the chamber midplane to measure the temperature drop across the specimen. Additional thermocouples were placed in the cylinder walls at the ends to monitor the axial gradient.

The chamber was positioned in a large environmental chamber and was surrounded by three 100-mm-diam independently controlled muffle heaters, as shown in Fig. 3. For each data point the temperatures of these three heaters were adjusted until the axial variation on the specimen chamber was less than 0.5 K.

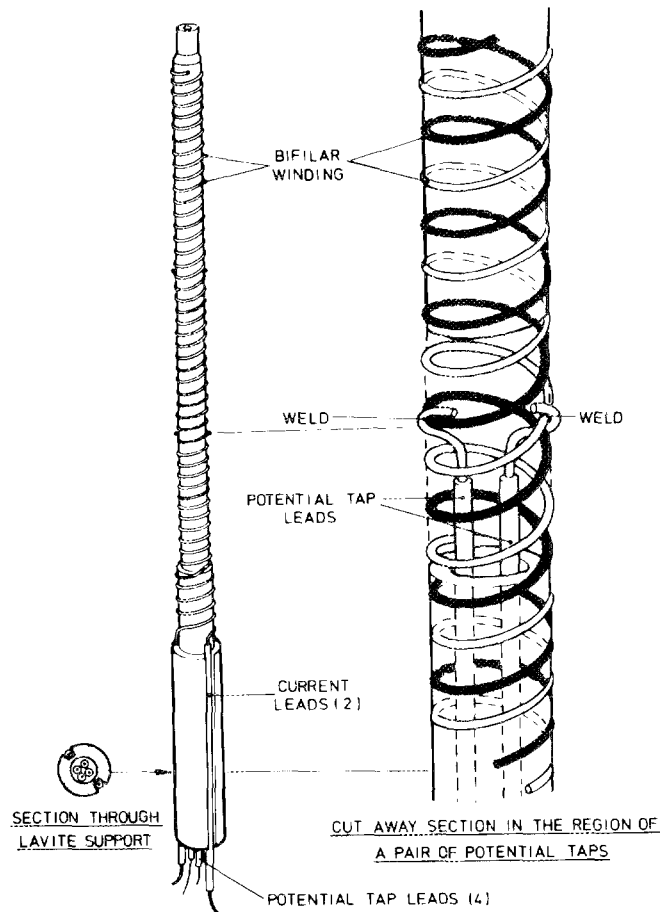


Fig. B1. Core heater for radial heat flow apparatus.

Joule heat was generated in the core heater by passing a regulated direct current through the platinum heater wire. The power generated per unit length was determined by measuring the voltage drops between the potential taps and across a standard resistor wired in series with the core heater windings. The heat output from the core heater was usually adjusted to yield a temperature drop of from 5 to 15 K across the specimen annulus. When the system reached steady state, the voltages from the thermocouples were measured with a six-dial potentiometer. After standardization, a precision of $0.01 \mu\text{V}$ could be achieved. The voltages on the core heater and the voltage drop across the standard resistor were measured with a less precise potentiometer because the greater accuracy of

the six-dial was not needed for these large signals. The thermocouple voltages were converted to temperature, and the thermal conductivity was calculated by using Eq. (A1) of Appendix A except that $T(r=0)$ was replaced with $T(r_5)$, where r_5 was now the distance from the system central axis to the thermocouple wells in the inner tube, and q' was determined from the voltage and current. The total determinate error for ORNL-2, based on an analysis similar to that given in Appendix A, was $\pm 3.2\%$.

Indeterminate errors in this system were similar to those discussed in Appendix A for ORNL-1. Thermal modeling showed that at 1050 K error due to nonradial heat flow at the specimen midplane would be +0.7%, +10%, and +20% for specimen conductivities of 1.5, 0.7, and 0.3 W/(m·K), respectively.

Measurements on a powder consisting of 500- μ m-diam spherical Al_2O_3 particles in nitrogen at a pressure of 0.1 MPa gave values of 0.3361, 0.4365, 0.4687, and 0.5222 W/(m·K) at temperatures of 414.5, 631.5, 721.9, and 887.4 K, respectively. These results are about 7% above calibration values obtained on this same powder in a chamber so large (90 mm diam \times 355 mm high) that it was not subject to many of the potential errors in ORNL-2. This positive deviation from the calibration values agrees with the prediction from the thermal modeling studies. For a system with such a small specimen volume this is a relatively low error.

Measurements in ORNL-2 made on samples of MgO powder gave results that were lower than those reported by previous workers,¹ but this difference may be due to a different specimen density.

Reference

1. H. W. Godbee, *Thermal Conductivity of Magnesia, Alumina, and Zirconia Powders in Air at Atmospheric Pressure from 200°F to 1500°F*, ORNL-3510, April 1966.

Appendix C

MODELS FOR HEAT CONDUCTION IN VIBRATORILY COMPACTED POWDERS WITH SPHERICAL PARTICLES

Models were derived for heat conduction in the vibratorily compacted specimens containing ThO_2 particles. One of the most important assumptions in all calculations was that the isotherms are parallel to the bounding surfaces of the specimen annulus.

C1. Model for Powders with a Single Size Particle

C1.1. Geometrical Model of Sphere Packing

We needed to construct a model for the packing of solid spheres that would yield the correct density. The model proposed by Shimokawa¹ was used to describe the beds containing single-size spheres.

Simple hexagonal packing of solid spheres was assumed. A projection onto the (010) plane is shown in Fig. C1(a) and a (001) plane projection in Fig. C1(b). The spheres are in contact, and the projections of the unit cell used for the calculation of thermal conductivity are outlined. A sketch of the unit cell in Fig. C2 shows a section parallel to the basal plane and an exploded view of the cell as a whole. One half [Fig. C2(c)] of the unit cell was further subdivided into the components shown in (d) and (e). Figure C2(f) is a section through the component shown in Fig. C2(d).

An analysis of the geometry pertaining to this unit cell (cell A) is given in Sect. C1.2, which shows that the solid fraction in this cell is 0.605. This is sufficiently near the values of 0.585 to 0.64 in the beds with single-size particles listed in Table 1 that this model may be used for the analysis.

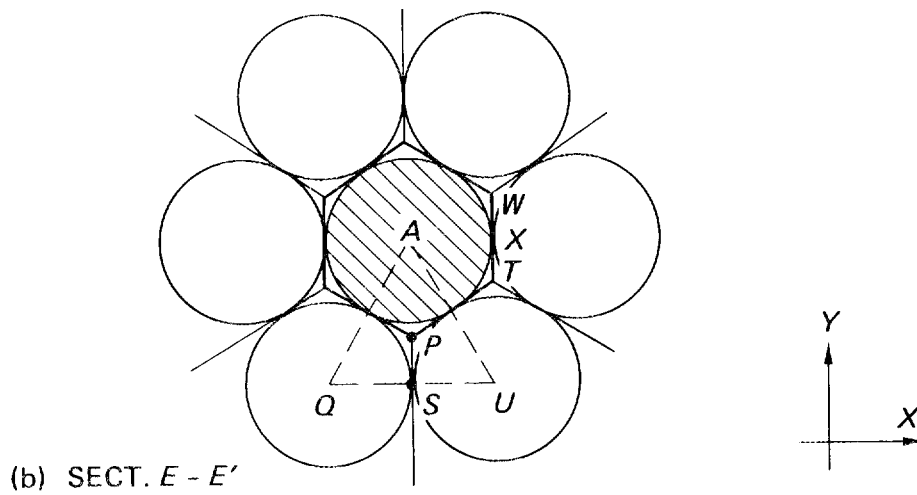
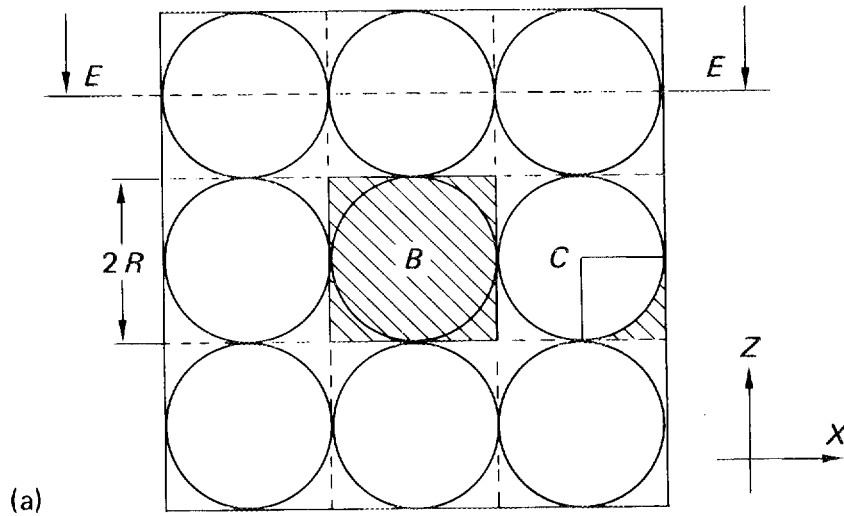


Fig. C1. Plane projections of the unit cell for a 60.5%-dense bed, showing (a) the projection onto the (010) plane and (b) the projection onto the (001) plane.

ORNL-DWG 82-7651

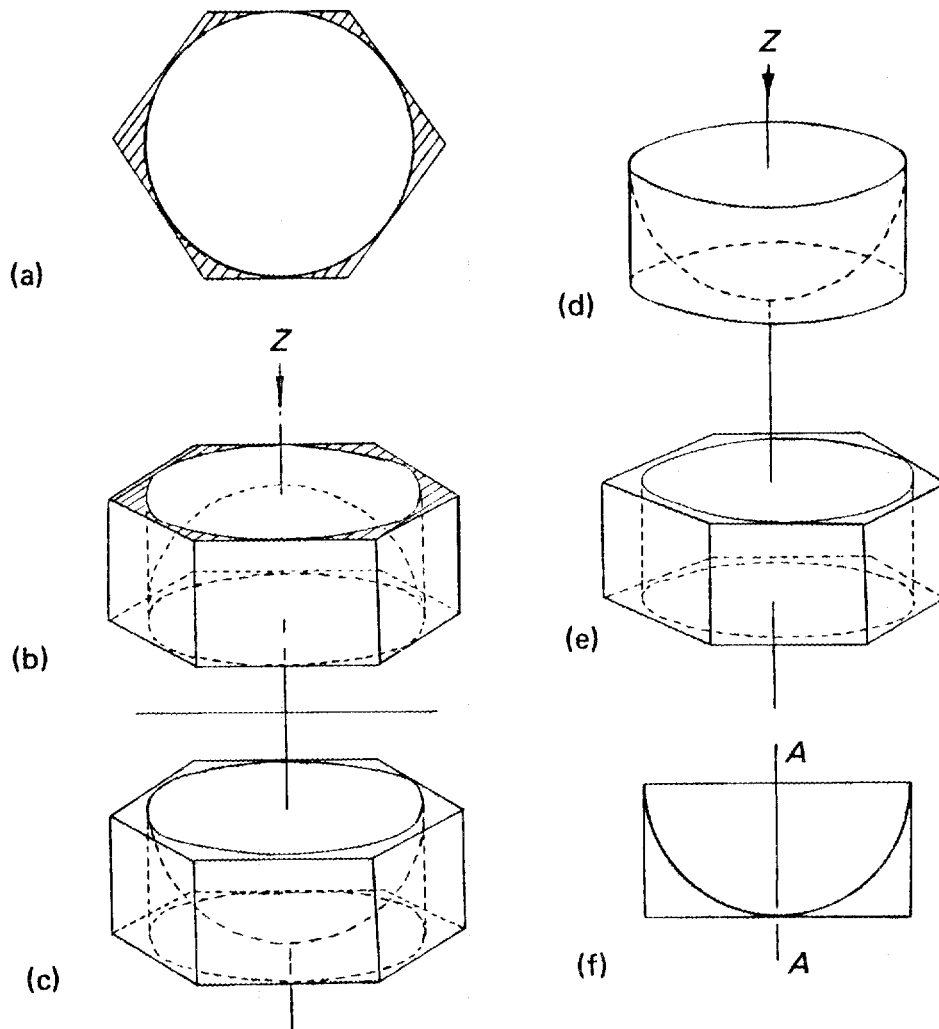


Fig. C2. Unit cell for a 60.5%-dense bed, showing (a) the basal plane projection, (b) and (c) exploded views of the unit cell, (d) the cylindrical component, (e) the hexagonal component, and (f) a section through the cylindrical component.

C1.2. Analysis of Unit Cell A

The volume of the unit cell is found from Fig. C1(b). In triangle AQU :

$$AQ = 2R.$$

$$QS = R.$$

$$\text{Therefore, } AS = \sqrt{3}R.$$

P is the center of gravity of triangle AQU .

$$\text{Therefore, } AP = (2/3)(\sqrt{3}R).$$

$$\text{Area of parallelogram } APTW = AP(AQ) = (2/3)(\sqrt{3}R)(2R) = (2/3)\sqrt{3}R^2.$$

$$\text{Total base area of unit cell} = 3(2/3)(\sqrt{3}R^2) = 2\sqrt{3}R^2.$$

$$\text{Volume of unit cell, } V_T = \text{base area} \times \text{height} = 2\sqrt{3}R^2(2R) = 4\sqrt{3}R^3.$$

$$\text{Volume of "cylinder-sphere" component [Fig. C2(d)], } V_C = \pi R^2(2R) = 2\pi R^3.$$

$$\text{Volume of solid in unit cell [Fig. C2(b), (c)] } V_S = (4/3)\pi R^3.$$

$$\text{Volume of "hexagonal-cylinder" component [Fig. C2(e)], } V_O = V_T - V_C = 2R^3(2\sqrt{3} - \pi).$$

$$\text{Volume fraction solid} = V_S/V_T = (4/3)\pi R^3/4\sqrt{3}R^3 = 0.605 = 60.5\%.$$

$$\text{Volume fraction of "cylinder-sphere" component, } f_{cy} = V_C/V_T = 2\pi R^3/4\sqrt{3}R^3 = 0.907.$$

$$\text{Volume fraction of "hexagonal-cylinder" component, } f_H = V_O/V_T = 2R^3(2\sqrt{3} - \pi)/4\sqrt{3}R^3 = 0.093.$$

C1.3 Model for the Calculation of Effective Thermal Conductivity

We assumed that heat flowed in the Z -direction (Fig. C2). The two components of the unit cell, "cylinder-sphere" component [Fig. C2(d)] and "hexagonal-cylinder" component [Fig. C2(e)], were treated separately as thermal resistances in parallel. The effective thermal conductivity of the unit cell was calculated as follows:

1. The effective thermal conductivity for conduction heat transfer in the "cylinder-sphere" component of the unit cell was determined. This was done by summing the effective thermal conductivities of parallel concentric cylinders. The thermal conductivity of each elemental cylinder in turn was determined by considering the gas and solid within such a cylinder as thermal resistances in series.

2. The effective thermal conductivity for conduction heat transfer in the "hexagonal-cylinder" component of the unit cell was determined.

3. The contribution of radiation heat transfer to each component was calculated.

4. The total effective thermal conductivity of the unit cell was determined by considering the two components as thermal resistances in parallel.

A schematic representation of the method is given in Fig. C3. The details of each calculation will next be considered.

ORNL-DWG 82-7652

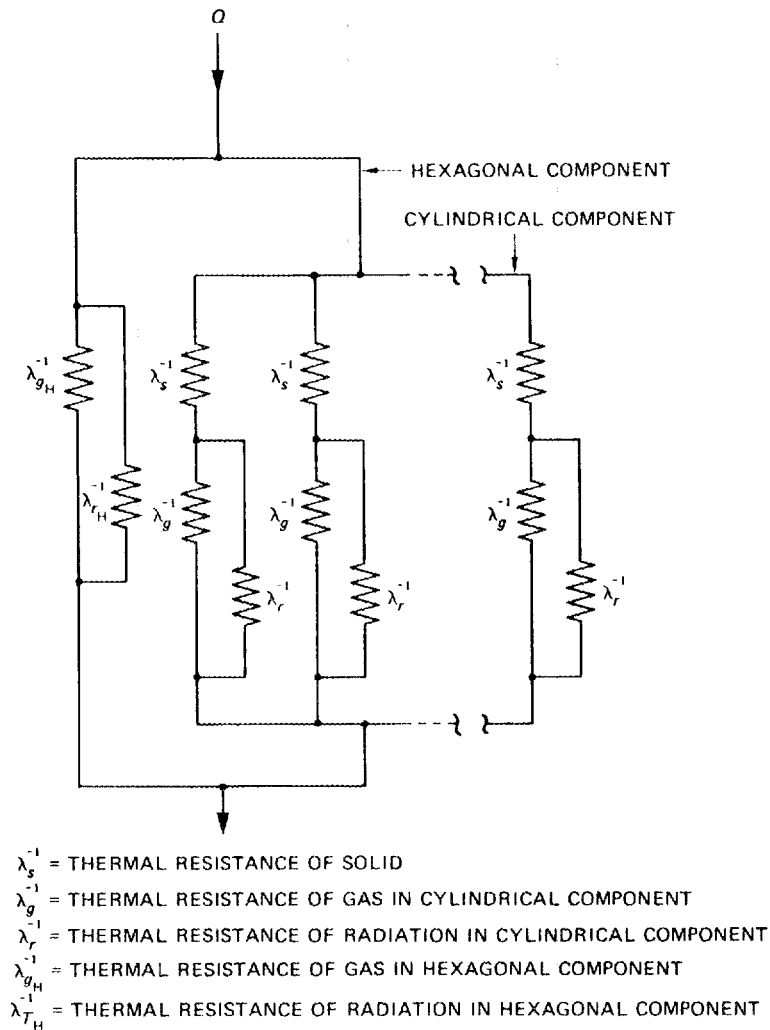


Fig. C3. Schematic analog of method used to determine the effective thermal conductivity of a 60.5%-dense bed.

Conduction Heat Transfer in "Cylinder-Sphere" Component. A section through one half of the unit cell is given in Fig. C2(f). Line A-A is a line of symmetry, so that it was necessary to analyze only one quarter of the "cylinder-sphere" component, and this section is shown in Fig. C4. The effective thermal conductivity of an elemental cylinder, distance Y from the center and of width W , was first calculated. The solid and gas within one such cylinder were considered as thermal resistances in series, because we assumed that the heat flow was perpendicular to the isotherms. The effective thermal conductivity of the elemental cylinder i was then given by

$$\lambda^i = \lambda_s \lambda_c^g / (f_s \lambda_c^g + f_c^g \lambda_s) \quad , \quad (C1)$$

where

λ^i = effective thermal conductivity of elemental cylinder i ,

λ_s = thermal conductivity of the solid,

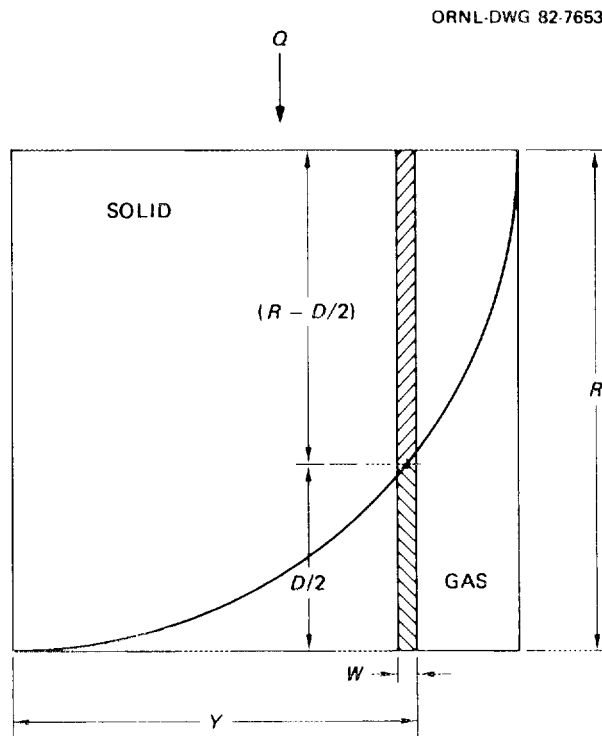


Fig. C4. One quarter of the cylindrical component of the unit cell for a 60.5%-dense bed.

- λ_c^g = thermal conductivity of the portion of gas in the elemental cylinder,
 f_s = solid fraction in elemental cylinder, and
 f_c^g = gas fraction in elemental cylinder.

The solid conductivity was found from known experimental values, and the solid and gas fractions were determined from the geometry of the system:

$$f_s = (R - D/2)/R \quad (C2)$$

$$f_c^g = (1 - f_s) = D/2R \quad (C3)$$

where

$$D = 2(R - \sqrt{R^2 - Y^2}) \quad (C4)$$

The conductivity of the gas had to be calculated because assumption of bulk properties for the gas in the space between the solids was not justified. Near the contact between the solid particles, the distance between the spheres approaches the mean free path of the gas molecules. Rarefied gas properties were therefore expected in this region, and the "temperature-jump" effect was considered.

Smoluchowski² and Knudsen³ have shown that a discontinuity of temperature occurs at a wall bounding an unequally heated gas. This situation is shown schematically in Fig. C5. The temperature gradient is dT/dx in the gas between walls A and B. However, the temperature measured at wall A was not T_K but T_w . The distance G (the temperature jump distance) is a measure of the discontinuity in temperature and was expressed by Eq. (A3) in Appendix A, which can be approximated with

$$T_K - T_w = G \Delta T/d \quad (C5)$$

where d is the distance between plates.

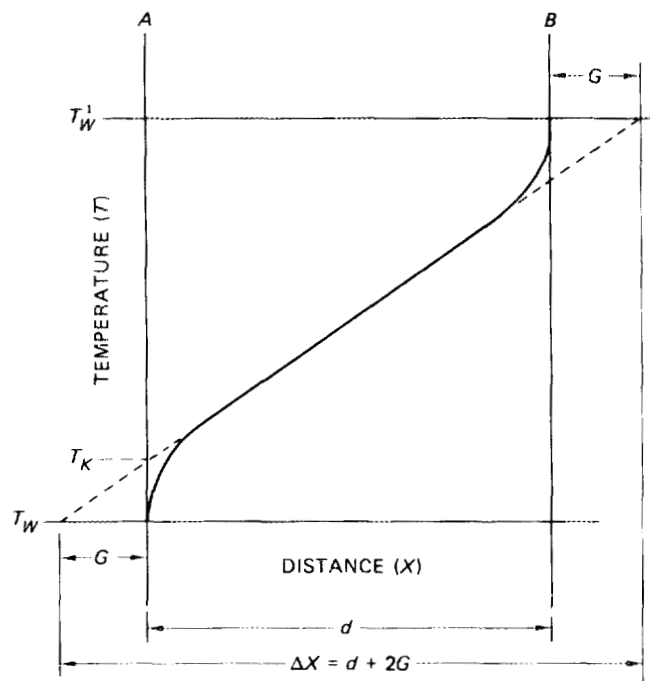


Fig. C5. Schematic illustration of the temperature-jump effect.

An expression for G in terms of properties is given as a variation of Eq. (A4) or

$$G = \frac{2 - \alpha}{\alpha} \frac{(2\pi RT)^{1/2}}{\gamma + 1} \frac{\lambda_g}{C_v P} \quad . \quad (C6)$$

where

R = gas constant,

T = absolute temperature,

P = pressure,

and the other constants have been defined in Appendix A.

When the temperature jump is small compared with the temperature difference between walls, the heat transferred by conduction between the two walls A and B distance d apart may be approximated with

$$q = \lambda_g A \Delta T / \Delta x \quad , \quad (C7)$$

where

- q = heat transferred from wall B to wall A,
 λ_g = thermal conductivity of the bulk gas,
 A = surface area,
 ΔT = temperature difference between the walls, and
 Δx = $(d + 2G)$ = effective distance between the walls if a linear temperature gradient is assumed. This is valid only if G is small compared with d .

Therefore,

$$q = \lambda_g A \Delta T / (d + 2G) \quad . \quad (C8)$$

An effective thermal conductivity of the gas between the two walls, λ_c^g , may be defined in analogy to Fourier's equation:

$$q = \lambda_c^g A \Delta T / d \quad . \quad (C9)$$

Combination of Eqs. (C8) and (C9) yields

$$\lambda_c^g = \frac{\lambda_g d}{d + 2G} = \frac{\lambda_g}{1 + 2G/d} \quad . \quad (C10)$$

Further consideration of Fig. C4 shows that the effective thermal conductivity of the gas in each elemental cylinder can be computed as a function of D , the distance between the spheres. This value was substituted in Eq. (C1), and the effective thermal conductivity of each elemental cylinder was then calculated.

Equation (C10) loses its validity in the region of contact between the spherical particles, and rarefied gas properties have to be considered when the distance D between the solid spheres is less than Λ , the mean free path of gas molecules. Kennard⁴ gives an expression for the heat

conduction between two parallel plates under rarefied gas conditions. A similar expression for the case under consideration is derived in Appendix D. This equation is

$$\lambda_e^{\text{RAR}} = \frac{\alpha(\gamma + 1)}{2(2 - \alpha)} \frac{C_v P D}{(2\pi RT)^{1/2}}, \quad (\text{C11})$$

where λ_e^{RAR} = effective thermal conductivity of the gas under rarefied conditions.

When $D < \Lambda$, Eq. (C11) was used to determine the effective thermal conductivity of the gas in each elemental cylinder. Constants used to calculate G and λ_e^{RAR} are given in Table F1 of Appendix F.

Conduction Heat Transfer in Hexagonal-Cylinder Component. The effective thermal conductivity of the gas in this space is given, in analogy to Eq. (C10), by

$$\lambda_H = \frac{\lambda_g}{1 + 2G/D} \quad (\text{C12})$$

where $D = 2R$.

Contribution of Radiation. The amount of heat transferred by radiation between two identical parallel plates⁴ can be expressed as

$$q = N_r^2 \sigma \Sigma A_r (T_1^4 - T_2^4), \quad (\text{C13})$$

where

N_r = refractive index of medium between surfaces,

σ = Stefan-Boltzmann constant,

Σ = emittance of radiating surfaces,

A_r = radiating surface area, and

T_1, T_2 = absolute temperatures of radiating surfaces.

The term containing the absolute temperatures can be written as $(T_1 - T_2)(T_1 + T_2)(T_1^2 + T_2^2)$. If we assume that $(T_1 + T_2) \approx 2T$ and $(T_1^2 + T_2^2) = 2T^2$, Eq. (C13) becomes

$$q = N_r^2 \sigma \Sigma A_r (T_1 - T_2) 4T^3 .$$

Therefore,

$$q = 4N_r^2 \sigma \Sigma A_r (\Delta T) T^3 . \quad (C14)$$

An effective thermal conductivity for radiation may be defined in analogy to Fourier's equation for the space between the two parallel surfaces, separated a distance D , and one obtains

$$q = \lambda_c^r A_r \Delta T / D . \quad (C15)$$

Combination of Eqs. (C14) and (C15) yields

$$\lambda_c^r = 4N_r^2 \sigma \Sigma T^3 D . \quad (C16)$$

The radiation contribution to the conductivity in the "hexagonal-cylinder" component is given by

$$\lambda_c^r = 4N_r^2 \sigma \Sigma T^3 (2R) . \quad (C17)$$

The effective thermal conductivity of the gas in each elemental cylinder in the "cylinder-sphere" component of the unit cell is therefore the sum of the conduction and radiation coefficients of thermal conductivity:

$$\lambda_e^g = \lambda_e^g + \lambda_e^r , \quad (C18)$$

where

- λ_e^g = total effective thermal conductivity of the gas in an elemental cylinder
- λ_e^g = thermal conductivity of gas space due to gas, and
- λ_e^r = radiation contribution to the total thermal conductivity.

A similar argument applies to the "hexagonal-cylinder" component of the unit cell.

Total Effective Thermal Conductivity of Cell A. The total effective thermal conductivity of cell A can now be determined by taking the thermal resistance of the "cylinder-sphere" component in parallel with that of the "hexagonal-cylinder" component. The total effective thermal conductivity of unit cell A can now be expressed as

$$\lambda_e^{TA} = f_{cy} \lambda_{cy} + f_H \lambda_H \quad , \quad (C19)$$

where

- λ_e^{TA} = total effective thermal conductivity of unit cell A,
- λ_{cy} = effective thermal conductivity of "cylinder-sphere" component,
- λ_H = effective thermal conductivity of "hexagonal-cylinder" component,
- f_{cy} = volume fraction of "cylinder-sphere" component, and
- f_H = volume fraction of "hexagonal-cylinder" component.

Section C1.2 shows that $f_{cy} = V_c/V_T = 0.907$ and $f_H = V_o/V_T = 0.093$.

The effective thermal conductivity in the cylindrical component can be written as

$$\lambda_{cy} = \sum_{i=1}^h (\lambda_e^i f^i) \quad , \quad (C20)$$

where

- h = number of elemental cylinders,
- λ_e^i = effective thermal conductivity of elemental cylinder, and
- f^i = volume fraction of elemental cylinder.

The last two quantities can be written as

$$f^i = [Y^2 - (Y - W)^2]/R^2 \quad (\text{Fig. C4}) \quad (C21)$$

and

$$\lambda_e^i = \frac{\lambda_s \lambda_e^g}{f_s \lambda_e^g + f_c^g \lambda_s} , \quad (C22)$$

where λ_e^g = effective thermal conductivity of gas with radiation taken into account (Eq. C18).

The effective thermal conductivity in the hexagonal component is

$$\lambda_H = \lambda_g / (1 + G/R) + \lambda_H^r , \quad (C23)$$

where λ_H^r = radiation contribution for the hexagonal component of the unit cell. The variables used in the computer program for calculating the thermal conductivity of the powder with a 60.5% loading are given in Appendix F and the program is listed in Appendix G.

C2. Model for the Two-Particle Compacted Bed of ThO₂ (Bed 7)

It will be recalled that the two-particle compacted bed of ThO₂ (bed 7) described in Table 1 was prepared by first vibratorily compacting particles with a diameter of 440 μm . Particles with diameters up to 44 μm were then infiltrated into the voids between large particles by further vibration. This simplified analysis assumed that all the small particles had diameters of 44 μm .

C2.1 Geometrical Model of Sphere Packing

We assumed that coarse microspheres (440 μm) were packed in a simple hexagonal mode. The fine microspheres (44 μm) were then stacked in the gas spaces left between the coarse spheres. We further assumed that the fine microspheres were in turn also stacked in a simple hexagonal array in the available space.

The composite unit cell, consisting of both 440- and 44- μm -diam microspheres, was subdivided in the same way as before, into "cylinder-sphere" and "hexagonal-cylinder" components [Fig. C2(d) and (e)].

Figure C6 is a section through the cylindrical component. To simplify the analysis, we assumed the coarse microsphere to be notched as shown. The gas space between the coarse particles could accommodate three vertical columns of small particle unit cells, as shown in Fig. C6.

Small microsphere unit cells can also be stacked in the gas space forming the "hexagonal-cylinder" component of the coarse particle unit cell as shown in Fig. C7(a). In this case we also assumed that the small particles were packed by putting a column of small particle unit cells into the available gas space.

A basal plane projection of a composite unit cell thus formed by coarse and fine microspheres is shown in Fig. C7(b). It is evident that close packing of hexagonal unit cells cannot be achieved in a cylindrical volume. For this reason gas columns, as shown in Fig. C6, were introduced to compensate for the gas volume not taken up by small unit cells.

ORNL-DWG 82-7655

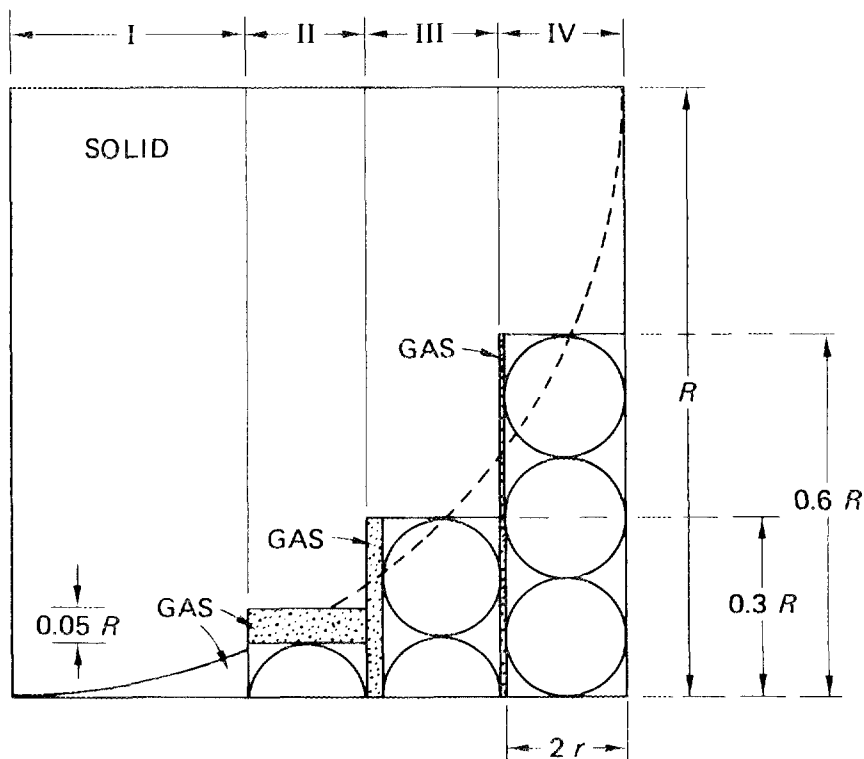
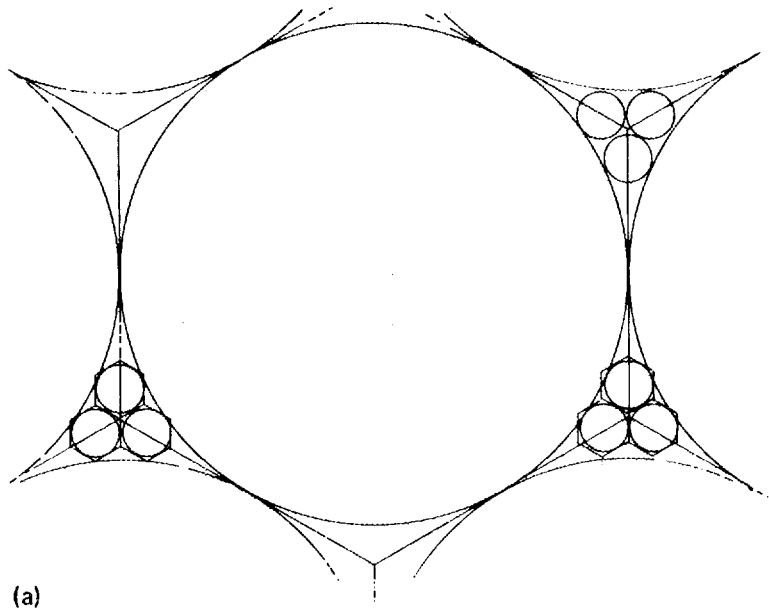
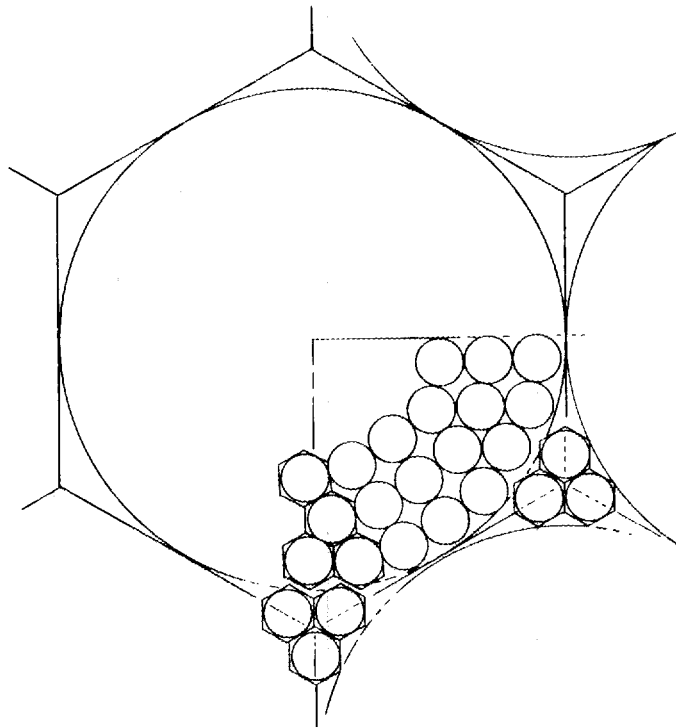


Fig. C6. Section through one quarter of the cylindrical component of the unit cell for an 80.5%-dense bed.



(a)



(b)

Fig. C7. Projections onto the basal plane of the unit cell for 80.5%-dense bed.

Geometrically some 270 small (44- μm -diam) unit cells can be packed in the "cylinder-sphere" component of a large (440- μm -diam) unit cell and 60 small unit cells in the "hexagonal-cylinder" component. A composite unit cell that was used for analyzing the heat transfer in beds of 84% solid density consists therefore of one 440- μm -diam particle and 330 particles with a diameter of 44 μm . Such a composite unit cell is geometrically analyzed in Sect. C2.2. The volume fraction of solid was calculated as 0.805, whereas that obtained for the two-particle compacted bed of ThO_2 (bed 7) was actually 0.84.

C2.2 Analysis of Unit Cell B

Volume of big unit cell (440- μm particle) =	$4\sqrt{3}R^3$
Volume of small unit cell (44- μm particle) =	$4\sqrt{3}(R/10)^3$
Number of small unit cells in column I (Fig. C6) =	0
Number of small unit cells in column II (Fig. C6) =	18
Number of small unit cells in column III (Fig. C6) =	72
Number of small unit cells in column IV (Fig. C6) =	180

Total of small unit cells in "cylinder-sphere" component (Figs. C6 and C7) of big unit cell =	270
Total number of small unit cells in "hexagonal-cylinder" component (Figs. C6 and C7) of big unit cell =	60

Therefore, total number of small unit cells in composite unit cell =	330
Volume of 44- μm -diam solid particles = $4\sqrt{3}(R/10)^3 \times 330 \times 0.605 =$	$1.3821R^3$
Volume of 440- μm -diam solid particles = $4\sqrt{3}R^3 \times 1 =$	$4.1888R^3$

Therefore, total solid volume in composite cell =	$5.5709R^3$
Volume fraction solid = $\frac{5.5709R^3}{6.9284R^3}$	
Therefore, volume fraction solid = 0.804 = 80.4%.	

C2.3 Analysis of the Thermal Conductivity in the Composite Unit Cell

Because of symmetry, we needed to consider only one quarter of the "cylinder-sphere" component of the unit cell, a section of which is shown in Fig. C6. This "cylinder-sphere" component was subdivided into four columns as shown. Each column (actually a cylinder) was treated separately as shown below.

Column I. For $0 < Y < 0.4R$ the analysis was done as in model A. That is, the effective thermal conductivities of elemental vertical cylinders were calculated and these cylinders were then treated as thermal resistances in parallel (Fig. C3). Therefore,

$$\lambda_e^I = \frac{l}{1} \sum (\lambda_e^i f^i) \quad , \quad (C24)$$

where

$$\begin{aligned} \lambda_e^I &= \text{effective thermal conductivity of cylinder I,} \\ l &= \text{number of elemental cylinders,} \\ \lambda_e^i &= \text{thermal conductivity of elemental cylinder, and} \\ f^i &= \text{volume fraction of elemental cylinder.} \end{aligned}$$

Column II. The thermal conductivity of the gas space (Fig. C6) was determined as before:

$$\lambda_c = \frac{\lambda_g}{1 + 2G/N} + \lambda_c \quad , \quad (C25)$$

where N is the length of the gas space and the other terms have been previously defined.

The thermal resistances of the solid and the gas space were taken in series, resulting in the expression

$$\lambda_e^{s-g} = \frac{\lambda_s \lambda_c^g}{f_s \lambda_g^c + f_c^g \lambda_s} \quad , \quad (C26)$$

where

$$\begin{aligned}\lambda_e^{s-g} &= \text{effective thermal conductivity of solid plus gas in} \\ &\quad \text{column II,} \\ \lambda_s &= \text{thermal conductivity of solid,} \\ f_s &= \text{volume fraction of solid, and} \\ f_c^g &= \text{volume fraction of gas.}\end{aligned}$$

The effective thermal conductivity of column II was then determined by taking $1/\lambda_e^{s-g}$ in series with the thermal resistance of the column of small (44 μm) unit cells, henceforth referred to as the composite. Therefore,

$$\lambda_e^{\text{II}} = \frac{\lambda_e^{s-g} \lambda_{\text{comp}}}{f_{s-g} \lambda_{\text{comp}} + f_{\text{comp}} \lambda_e^{s-g}}, \quad (\text{C27})$$

where

$$\begin{aligned}\lambda_e^{\text{II}} &= \text{effective thermal conductivity of column II,} \\ \lambda_{\text{comp}} &= \text{effective thermal conductivity of composite (column of} \\ &\quad \text{44-}\mu\text{m-diam unit cells),} \\ f_{s-g} &= \text{volume fraction of solid plus gas in column II, and} \\ f_{\text{comp}} &= \text{volume fraction of composite.}\end{aligned}$$

The thermal conductivity of a column of small (44- μm -diam) unit cells, λ_{comp} , was determined by the analysis on unit cell A.

Column III. The thermal resistances of the composite and gas space in this column were considered as being in parallel (Fig. C6). The effective thermal conductivity of the gas plus composite was then given by

$$\lambda_e^{g-c} = f_c^g \lambda_c^g + f_{\text{comp}} \lambda_{\text{comp}}, \quad (\text{C28})$$

where

$$\begin{aligned}\lambda_e^{g-c} &= \text{effective thermal conductivity of gas plus composite,} \\ \lambda_c^g &= \text{effective thermal conductivity of gas,} \\ \lambda_{\text{comp}} &= \text{effective thermal conductivity of composite,}\end{aligned}$$

$$\begin{aligned} f_c^g &= \text{volume fraction of gas, and} \\ f_{\text{comp}} &= \text{volume fraction of composite.} \end{aligned}$$

The effective thermal conductivity of the gas, λ_e^g , was determined from Eq. (C25). To determine the final effective thermal conductivity, we took the thermal resistance $1/\lambda_e^{g-c}$ in series with the thermal resistance of the solid, obtaining the expression

$$\lambda_e^{\text{III}} = \frac{\lambda_e^{g-c} \lambda_s}{f_s \lambda_e^{g-c} + f_{g-c} \lambda_s}, \quad (\text{C29})$$

where

$$\begin{aligned} \lambda_e^{\text{III}} &= \text{effective thermal conductivity of column III,} \\ \lambda_s &= \text{solid conductivity,} \\ f_s &= \text{volume fraction of solid, and} \\ f_{g-c} &= \text{volume fraction of gas plus composite.} \end{aligned}$$

Column IV. The effective thermal conductivity of column IV was determined in the same way as was that of column III.

"Hexagonal-Cylinder" Component of Unit Cell (Column V). The hexagonal component of the unit cell consists of columns of small (44- μm -diam) unit cells and gas. The effective thermal conductivity of this hexagonal component was determined by taking the thermal resistance of the composite (columns of small unit cells) in parallel. This treatment led to

$$\lambda_e^{\text{V}} = f_c^g \lambda_e^g + f_{\text{comp}} \lambda_{\text{comp}} \quad (\text{C30})$$

where

$$\begin{aligned} \lambda_e^{\text{V}} &= \text{effective thermal conductivity of hexagonal component,} \\ \lambda_e^g &= \text{effective thermal conductivity of gas,} \\ \lambda_{\text{comp}} &= \text{effective conductivity of composite,} \\ f_c^g &= \text{volume fraction of gas, and} \\ f_{\text{comp}} &= \text{volume fraction of composite.} \end{aligned}$$

Effective Thermal Conductivity of Unit Cell B. The effective thermal conductivity of the whole unit cell was finally determined by taking the thermal resistances of the five columns in parallel, which led to

$$\lambda_e^{TB} = f_1 \lambda_e^I + f_2 \lambda_e^{II} + f_3 \lambda_e^{III} + f_4 \lambda_e^{IV} + f_5 \lambda_e^V, \quad (C31)$$

where

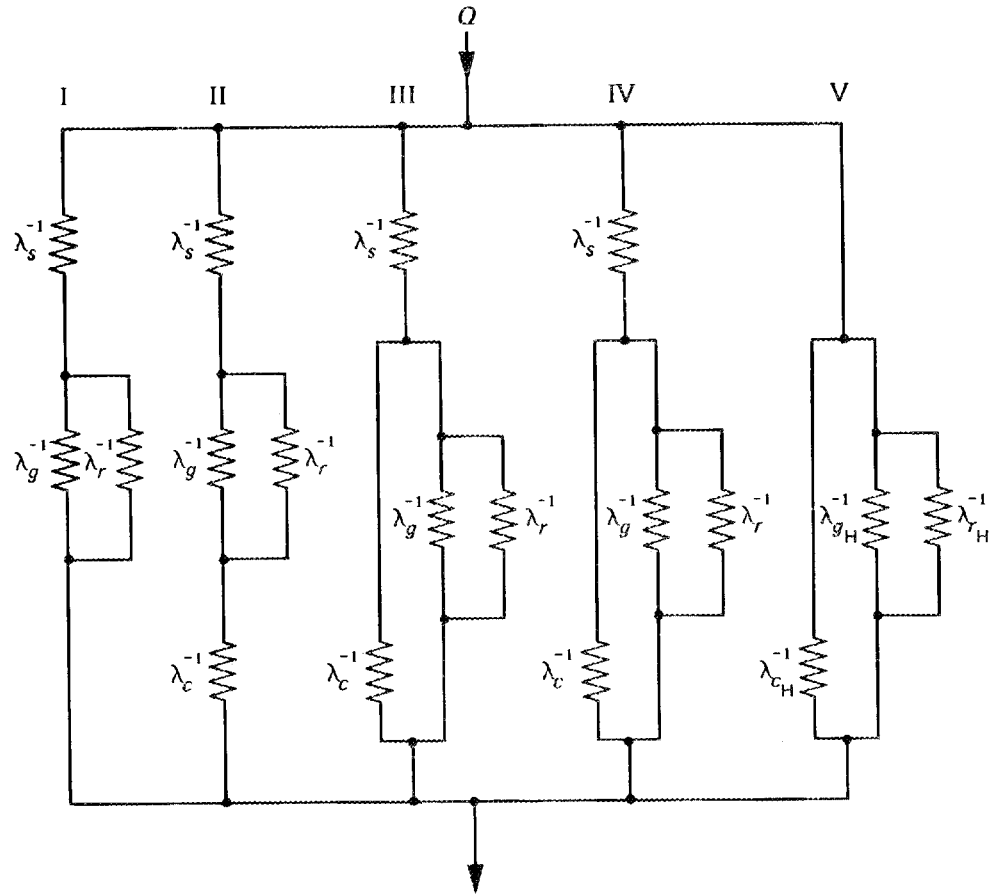
$$\begin{aligned} \lambda_c^{TB} &= \text{effective thermal conductivity of unit cell B,} \\ \lambda_e^i &= \text{effective thermal conductivity of column } i, \text{ and} \\ f_i &= \text{volume fraction of column } i. \quad (i = 1, 2, \dots, 5) \end{aligned}$$

A schematic analog of the method used is given in Fig. C8, and a numerical analysis of the volume fractions for unit cell B is given in Appendix E.

The variables used in the computer program for calculating the thermal conductivity of this powder with a total loading of 80.5% are given in Appendix F and the computer program is given in Appendix H.

References

1. J. Shimokawa, *Deionizing Processes with Ion Exchange and with Electromigration*, JAERI-1038, Japan Atomic Energy Research Institute, Tokyo, June 30, 1962.
2. M. S. Smoluchowski, *Philos. Mag.* 21: 11 (1911).
3. M. Knudson, *Ann. Phys. (Leipzig)* 34: 593 (1911).
4. E. H. Kennard, *Kinetic Theory of Gases*, McGraw-Hill, New York, 1938.



λ_s^{-1} = THERMAL RESISTANCE OF SOLID

λ_g^{-1} = THERMAL RESISTANCE OF GAS

λ_r^{-1} = THERMAL RESISTANCE OF RADIATION

λ_c^{-1} = THERMAL RESISTANCE OF COMPOSITE

λ_{gH}^{-1} = THERMAL RESISTANCE OF GAS IN HEXAGONAL COMPONENT

λ_{rH}^{-1} = THERMAL RESISTANCE OF RADIATION IN HEXAGONAL COMPONENT

λ_{cH}^{-1} = THERMAL RESISTANCE OF COMPOSITE IN HEXAGONAL COMPONENT

Fig. C8. Schematic analog of the method used to determine the effective thermal conductivity of the unit cell for the 80.5%-dense bed.

Appendix D

EXPRESSION FOR THE THERMAL CONDUCTIVITY OF A RAREFIED GAS

Smoluchowski¹ and Knudsen² have derived expressions for the thermal conductivity of a rarefied gas, but the notation of Kennard³ will be used. The heat transferred per unit area between two identical parallel plates (where the distance between the plates is smaller than the mean free path of a gas) can be expressed as

$$\frac{q}{A} = \frac{\alpha(\gamma + 1)}{2(2 - \alpha)} \frac{C_v P^* (T_1 - T_2)}{2\pi R T^*}, \quad (D1)$$

where

T_1 = temperature of one plate,

T_2 = temperature of the other plate,

P^* = $P\sqrt{T^*/T}$,

P^* = pressure of gas at temperature T^* ,

T^* is defined by $1/\sqrt{T^*} = (1/\sqrt{T_1^*} + 1/\sqrt{T_2^*})/2$,

$T_1^* = [T_1 + (1 - \alpha)T_2]/(2 - \alpha)$, $T_2^* = [T_2 + (1 - \alpha)T_1]/(2 - \alpha)$,
and the other terms have been defined previously.

If the temperature difference between the plates, ΔT , is small,

$$P^* \approx P$$

and

$$T^* \approx T = (T_1 + T_2)/2 .$$

Equation (D1) then becomes

$$\frac{q}{A} = \frac{\alpha(\gamma + 1)}{2(1 - \alpha)} \frac{C_v P}{(2\pi R T)^{1/2}} (\Delta T) . \quad (D2)$$

An effective thermal conductivity for the gas between the two plates, distance D apart, may be defined as

$$q/A = \lambda_e^{\text{RAR}} \Delta T/D \quad . \quad (\text{D3})$$

From Eq. (D2) and Eq. (D3),

$$\lambda_e^{\text{RAR}} = \frac{\alpha(\gamma + 1)}{2(2 - \alpha)} \frac{C_v PD}{(2\pi RT)^{1/2}} \quad . \quad (\text{D4})$$

References

1. M. S. Smoluchowski, *Philos. Mag.* 21: 11 (1911).
2. M. Knudson, *Ann. Phys. (Leipzig)* 34: 593 (1911).
3. E. H. Kennard, *Kinetic Theory of Gases*, McGraw-Hill, New York, 1938.

Appendix E

Volume for Constituents of Composite Unit Cell (Cell B)
from Figs. C2, C6, and C7

	I $\times R^3$	II $\times R^3$	III $\times R^3$	IV $\times R^3$	V "Hexagonal- cylinder" $\times R^3$
440- μm solid microsphere	0.9474	1.0668	1.2524	0.9222	
Small unit cells in "cylinder-sphere" portion of composite cell	0	0.1247	0.4988	1.2471	
Gas in "cylinder-sphere" portion of composite cell	0.1044	0.0658	0.0237	0.0299	
Small unit cells in "hexagonal-cylinder" portion of composite cell					0.4157
Gas in "hexagonal-sphere" portion of composite cell					0.2295
Total volume of column	1.0518	1.2573	1.7749	2.1992	0.6452
Volume fraction of column	0.1518	0.1815	0.2562	0.3174	0.0931

Numerical Evaluation of Volume Fractions in Unit Cell B for Column II

$$\lambda_g^e = \frac{\lambda_g}{1 + 2G/0.05R} + 4N_T^2 \sigma \Sigma T^3 (0.05R)$$

$$\lambda_e^{s-g} = \frac{\lambda_s \lambda_g^e}{f_s \lambda_g^e + f_g^e \lambda_s}$$

$$f_s = \frac{1.0668}{1.0668 + 0.0658} = 0.9419$$

$$f_g^e = 1 - f_s = 0.0581$$

$$\lambda_e^{\text{II}} = \frac{\lambda_e^{s-g} \text{comp}}{f_{\text{comp}} \lambda_e^{s-g} + f_{s-g} \lambda_{\text{comp}}}$$

$$f_{s-g} = \frac{1.0668 + 0.0658}{1.0668 + 0.0658 + 1.247} = 0.9008$$

$$f_{\text{comp}} = 1 - f_{s-g} = 0.0992 \quad .$$

For Column III

$$\lambda_e^{g-c} = f_c^g \lambda_c^g + f_{\text{comp}} \lambda_{\text{comp}}$$

$$\lambda_c^g = \frac{\lambda_g}{1 + 2G/0.3R} + 4N_r^2 \sigma \Sigma T^3 (0.3R)$$

$$f_c^g = \frac{0.0237}{0.0237 + 0.4988} = 0.0454$$

$$f_{\text{comp}} = 1 - f_c^g = 0.9546 \quad .$$

$$\lambda_e^{\text{III}} = \frac{\lambda_e^{g-c} \lambda_s}{f_s \lambda_e^{g-c} + f_{g-c} \lambda_s}$$

$$f_s = \frac{1.2524}{1.2524 + 0.4988 + 0.0237} = 0.7056$$

$$f_{g-c} = 1 - f_s = 0.2944 \quad .$$

For Column IV

$$\lambda_e^{g-c} = f_c^g \lambda_c^g + f_{\text{comp}} \lambda_{\text{comp}}$$

$$\lambda_c^g = \frac{\lambda_g}{1 + 2G/0.6R} + 4N_r^2 \sigma \Sigma T^3 (0.6R)$$

$$f_{\text{comp}} = \frac{1.2471}{1.2471 + 0.0299} = 0.9766$$

$$f_c^g = 1 - f_{\text{comp}} = 0.0234$$

$$\lambda_c^{\text{IV}} = \frac{\lambda_e^{g-c} \lambda_s}{f_s \lambda_e^{g-c} + f_{g-c} \lambda_s}$$

$$f_s = \frac{0.9222}{0.9222 + 1.2471 + 0.0299} = 0.4193$$

$$f_{g-c} = 1 - f_s = 0.5807 \quad .$$

For Column V

$$\lambda_e^{\text{V}} = f_c^g \lambda_c^g + f_{\text{comp}} \lambda_{\text{comp}}$$

$$\lambda_c^g = \frac{\lambda_g}{1 + 2G/R} + 4N_r^2 \sigma \Sigma T^3 R$$

$$f_c^g = \frac{0.2295}{0.2295 + 0.4157} = 0.3557$$

$$f_{\text{comp}} = 1 - f_c^g = 0.6443 \quad .$$

Total Effective Thermal Conductivity of Cell B

$$\lambda_e^T = f_I \lambda_e^I + f_{II} \lambda_e^{II} + f_{III} \lambda_e^{III} + f_{IV} \lambda_e^{IV} + f_V \lambda_e^V .$$

Therefore,

$$\lambda_e^T = 0.1518 \lambda_e^I + 0.1815 \lambda_e^{II} + 0.2562 \lambda_e^{III} + 0.3174 \lambda_e^{IV} + 0.0931 \lambda_e^V .$$

Appendix F

NUMERICAL EVALUATION OF THE EFFECTIVE THERMAL CONDUCTIVITY FOR 60.5%- AND 80.5%-DENSE BEDS

Constants used in Eqs. (C6) and (C11) for calculating the temperature jump distance and the effective heat transfer between two parallel plates separated a distance less than G are given in Table F1 for argon, helium, and nitrogen.

Tables F2 and F3 describe the variables used in the computer programs, which are given in Appendices G and H, for calculating the powder thermal conductivity.

Table Fl. Constants used in the calculations of temperature jump and heat transfer in rarefied regions

Gas	C_p [J/(kg·K)]	M	R^a [J/(kg·K)]	C_v^b [J/(kg·K)]	γ^c	Γ^d (m ² ·K ^{1/2} ·Pa/W)	Λ (m)	θ^e (W/Pa·m·K ^{1/2})
Argon	519	39.944	208.4	311	1.669	4.3×10^{-2}	6.7×10^{-8}	7.7×10^{-7}
Helium	519	4.003	1261	3929	1.321	1.35×10^2	1.9×10^{-7}	9.7×10^{-6}
Nitrogen	1100	28.01	297.1	800	1.37	1.6×10^2	7.0×10^{-8}	1.5×10^{-6}

$$a_R = 8323/M \text{ (J/kg·K)}.$$

$$b_{C_v} = C_p - R.$$

$$c_\gamma = C_p/C_v.$$

$$d_G = \Gamma T^{1/2} \lambda_g / P \text{ where } \Gamma = (2\pi R)^{1/2} / (\gamma + 1) C_p;$$

$$e_{\lambda_{RAR}} = \theta P \alpha / (2 - \alpha) T^{1/2}, \text{ where } \theta = C_v (\gamma + 1) \Lambda / 2 (2\pi R)^{1/2}.$$

Table F2. Description of terms used to calculate the thermal conductivity of powder with a single size particle and program location of the term

Line	Variable	Text notation	Term definition
1.06	RP	—	Particle diameter
	E1	Σ	Emittance
1.08	RP	R	Particle radius (redefinition of RP)
	N	N	Number of regions for use of rarefied equations
1.10	V	Γ	Constant in Eq. (C5) ^a and Table F1
	C2	θ	Constant in Eq. (C11) ^a and Table F1
	Pr	P	Pressure in atmospheres
1.20	X	T	Absolute temperature (K)
	SC	λ_s	Solid conductivity
	BGC	λ_g	Bulk gas conductivity
1.30	A	α	Thermal accommodation coefficient
2.01	G	G	Temperature jump distance
2.10	W	W	Thickness of elemental cylinder (Fig. C4)
2.20	R	R	Radius of thoria sphere
3.01	Y	Y	Distance of elemental cylinder from center of unit cell (Fig. C4)
3.31	KFR	f^i	Volume fraction of elemental cylinder
	D	D	Distance between solid spheres (Fig. C4)
3.70	GFR	f_c^g	Gas fraction in elemental cylinder
3.70	SFR	f_s	Solid fraction in elemental cylinder
3.70	GC	λ_c^g	Effective gas thermal conductivity in elemental cylinder
3.92	CC	λ_e^i	Effective thermal conductivity of elemental cylinder
	ETC	$\lambda_e^{if^i}$	
	TH	λ_{cy}	Effective thermal conductivity of cylindrical component
4.01	P	λ_e^{TA}	Thermal conductivity of unit cell

^aThe values of these constants are in metric units in Table F1 but are adjusted in the computer programs so that P can be entered in atmospheres and the particle diameter can be entered in micrometers.

Table F3. Description of terms used to calculate the thermal conductivity of powders containing 440- μm -diam particles, 44- μm -diam particles, and a combination of the two sizes

Line	Variable	Text notation	Term definition
4.01	P	λ_e^{TA}	Effective thermal conductivity of unit cell A containing spheres 44 μm in diameter
7.10	Q	λ_e^{TA}	Effective thermal conductivity of unit cell A containing spheres 440 μm in diameter
8.10	L1	λ_c^g	Effective thermal conductivity of gas in column I cell B
8.20	L2	λ_c^g	Effective thermal conductivity of gas in column II cell B
8.30	L3	λ_c^g	Effective thermal conductivity of gas in column III cell B
8.40	L4	λ_c^g	Effective thermal conductivity of gas in column IV cell B
9.10	M1	λ_e^{s-g}	Equation (C21)
	E1C	λ_e^{II}	Equation (C22)
9.20	M2	λ_e^{g-c}	Equation (C23)
10.20	E2C	λ_e^{III}	Equation (C24)
11.10	M3	λ_e^{g-c}	Equation (C23) applied to column IV
11.10	E3C	λ_e^{IV}	Equation (C24) applied to column IV
11.20	E4C	λ_e^{V}	Equation (C25)
13.10	TC	λ_e^{TB}	Equation (C26) = effective thermal conductivity of cell B containing 440- and 44- μm -diam microspheres

Appendix G

COMPUTER PROGRAM IN FOCAL LANGUAGE* FOR CALCULATING THE THERMAL
CONDUCTIVITY OF POWDERS WITH A SINGLE SIZE SPHERICAL PARTICLE

C-FOCAL.J4.CODASIII 33534W

```

01.01 C THERMAL COND OF MONO SIZE MICROSPHERE PWDR ;MOORE 1981
01.02 C ENTER COND IN W/M-K,PRESSURE IN ATMOS,PART DIA IN MICRO-M
01.03 C S CONST V = 13.54,43.0,21.9*E-6 FOR HE,AR,N2,RESPECTIVELY
01.04 C S CONST C2=0.970,0.077,0.150 FOR HE,AR,N2,RESPECTIVELY
01.06 A "PARTICLE DIA",RP,"EMITTANCE",E1;T !
01.07 C CALC PARTICLE RADIUS & THE # OF INTERVALS FOR TINY GAPS (N)
01.08 S RP=RP/2.0;S N=0.34*FSQT(2.0*RP);T "N=";T %3.01,N;T " "
01.10 A "CONST V & C2 =",V,C2,"PRESSURE=";PR;T !
01.20 A "TEMP",X,"SOLID COND",SC,"GAS COND=";BGC;T !
01.30 A "ACC COEF",A;T !
01.40 T "ACC COEF=";T %4.02,A;T !

02.01 S G=(V*((2-A)/A)*BGC*(FSQT(X)))/PR
02.10 S W=1*0.0001
02.20 S R=RP*0.0001
02.31 S C=0;S TH=0
02.40 F I=1,RP;D 3.0
02.50 G 4.01

03.01 S Y=C+W;S C=Y;S H=Y-W
03.31 S KFR=(C*C-H*H)/(R*R);S D=2*(R-FSQT(R^2-Y*Y))
03.70 S GFR=D/R*2;S SFR=1-GFR
03.75 C GO TO RAREFIED GAS REGION AT CENTER OF PARTICLE FOR "N" SPACES ?
03.81 I (I-N)3.82,3.82,3.84
03.82 S GC=((C2*(A/(2-A))*PR)/(FSQT(X)))+22.68E-10*E1*D*X^3
03.83 G 3.92
03.84 S HC=BGC/(1+(2*G)/D)
03.91 S GC=BGC/(1+(2*G)/D)+22.68E-10*E1*D*X^3
03.92 S CC=(GC*SC)/(SC*GFR+GC*SFR);S ETC=CC*KFR;S ETC=ETC+TH;S TH=ETC

04.01 S P=TH*.907+.093*(HC+22.68E-10*2.0*E1*R*X^3)

05.01 T " COND OF ";T %6.02,2.0*RP;T %6.04,P
05.10 T !!;S A=A+0.1;G 1.40

31.98 W 1.01,!
31.99 L R 127;G 2.20
*
```

*DEC™ PDP-8e computer language modified to become CODASIII at ORNL.

Appendix H

COMPUTER PROGRAM IN FOCAL LANGUAGE FOR CALCULATING THE THERMAL
CONDUCTIVITY OF POWDERS WITH 440- μm -DIAM PARTICLES,
44- μm PARTICLES, AND A COMBINATION OF THE TWO SIZES

C-FOCAL.J4.CODASIII 33534W

```

01.01 C - THERMAL COND. OF POWDER;RIAN D. 1974. FILE 106.
01.02 C ENTER COND IN W/M'K,PRESSURE IN ATMOS
01.03 C SET CONST=13.54,43.0,21.9E-6 FOR HE,AR,&N2,RESPECTIVELY
01.04 C S CONST C2=0.970,0.077,0.150 FOR HE,AR,NE,RESPECTIVELY
01.06 A "EMITTANCE",E1;T !
01.10 A "CONST V & C2=",V,C2,"PRESSURE",PR;T !
01.20 A "TEMP",X,"SOLID COND",SC,"GAS COND",BGC;T !
01.30 A "ACC COEF",A;T !
01.40 T "ACC COEF=";T %4.02,A;T !
01.50 I (A-1)2.01,2.01,Q

02.01 S G=(V*((2-A)/A)*BGC*(FSQT(X)))/PR
02.10 S W=1*0.0001;S R=22*0.0001;S C=0;S TH=0;S N=2
02.40 F I=1,22;D 3.0
02.50 G 4.01

03.01 S Y=C+W;S C=Y;S H=Y-W
03.31 S KFR=(C*H)/(R*R);S D=2*(R-FSQT(R^2-Y*Y))
03.70 S GFR=D/R^2;S SFR=1-GFR
03.75 C GO TO RAREFIED GAS REGION AT CENTER OF PARTICLE FOR "N" SPACES ?
03.81 I (I-N)3.82,3.82,3.84
03.82 S GC=((C*(A/(2-A))*PR)/(FSQT(X)))+22.68E-10*E1*D*X^3
03.83 G 3.92
03.84 S HC=BGC/(1+(2*G)/D);S GC=BGC/(1+(2*G)/D)+22.68E-10*D*E1*X^3
03.92 S CC=(GC*SC)/(SC*GFR+GC*SFR);S ETC=CC*KFR;S ETC=ETC+TH;S TH=ETC

04.01 S F=TH*.907+.093*(HC+22.68E-10*E1*.0044*X^3)

05.01 T " " ,"TH. COND OF 44MIC.", " " " ,Z,P,!
05.02 S C=0;S Y=0;S TH=0;S N=7

06.02 S R=220*.0001;S W=1*0.0001
06.05 F I=1,220;D 3.0
06.06 G 7.10

07.10 S Q=TH*.907+.093*(HC+22.68E-10*E1*.044*X^3)
07.20 T " " ,"TH. COND OF 440MIC.", " " " ,Z,Q,!
07.21 S C=0;S W=.0001;S Y=0;S TH=0
07.30 F I=1,90;D 3
07.40 G 8.10

08.10 S L1=BGC/(1+2*G/(R*.05))+22.68E-10*E1*.0011*X^3
08.20 S L2=BGC/(1+2*G/(R*.3))+22.68E-10*E1*.0066*X^3
08.30 S L3=BGC/(1+2*G/(R*.6))+22.68E-10*E1*.0132*X^3
08.40 S L4=BGC/(1+2*G/R)+22.68E-10*E1*.044*X^3

```

```
09.10 S M1=SC*L1/(SC*.0581+L1*.9419);S E1C=M1*F/(M1*.0992+F*.9008)
09.20 S M2=P*0.9546+L2*.0454;S E2C=SC*M2/(SC*.2944+M2*.7056)

11.10 S M3=L3*.0234+F*.9766;S E3C=SC*M3/(M3*.4193+SC*.5807)
11.20 S E4C=L4*0.3557+F*0.6443

13.10 S TC=TH*.1518+E1C*.1815+E2C*.2562+E3C*.3174+E4C*.0931
13.20 T " " "TH. COND OF 440/44MIC." " " "Z,TC,!
13.30 T !!!;S A=A+0.2;G 1.40
```

INTERNAL DISTRIBUTION

- | | |
|------------------------------------|--------------------------------------|
| 1-2. Central Research Library | 16. A. L. Lotts |
| 3. Document Reference Section | 17-21. D. L. McElroy |
| 4-5. Laboratory Records Department | 22-26. J. P. Moore |
| 6. Laboratory Records, ORNL RC | 27. A. R. Olsen |
| 7. ORNL Patent Section | 28. A. L. Bement, Jr. (Consultant) |
| 8. A. J. Caputo | 29. E. H. Kottcamp, Jr. (Consultant) |
| 9-11. M. R. Hill | 30. Alan Lawley (Consultant) |
| 12. M. J. Kania | 31. T. B. Massalski (Consultant) |
| 13. W. J. Lackey | 32. R. H. Redwine (Consultant) |
| 14. Jar-Shyong Lin | 33. K. M. Zwilsky (Consultant) |
| 15. E. L. Long, Jr. | |

EXTERNAL DISTRIBUTION

- 34-38. R. J. Dippenaar, Materials Science Department, University of South Africa, Pretoria
- 39-44. R.O.A. Hall, Chemistry Division, AERE Harwell, Oxfordshire, England
- 45-51. DOE, DIVISION OF MATERIALS SCIENCES, Washington, DC 20545
- R. J. Gottschall
L. C. Ianniello
J. S. Kane
F. V. Nolfi
D. K. Stevens
M. C. Wittels
S. Wolfe
52. DOE, OAK RIDGE OPERATIONS OFFICE, P.O. Box E, Oak Ridge, TN 37830
Office of Assistant Manager for Energy Research and Development
- 53-259. DOE, TECHNICAL INFORMATION CENTER, Office of Information Services,
P.O. Box 62, Oak Ridge, TN 37830
- For distribution as shown in TID-4500 Distribution Category,
UC-25 (Materials)